공학석사학위논문

Development of land cover classification model using CNN based FusionNet network and parcel boundary extraction algorithm

CNN기반의 FusionNet 신경망과 농지 경계추출 알고리즘을 이용한 토지피복분류모델 개발

2021년 2월

서울대학교 대학원
생태조경·지역시스템공학부
지역시스템공학전공
박 진 석

Development of land cover classification model using CNN based FusionNet network and parcel boundary extraction algorithm

A THESIS

SUBMITTED TO THE DEPARTMENT OF LANDSCAPE ARCHITECTURE AND RURAL SYSTEMS ENGINEERING AND THE COMMITTEE ON GRADUATE STUDIES OF SEOUL NATIONAL UNIVERSITY IN PARTIAL FULFILLMENT OF THE REQUIREMENTS FOR THE DEGREE OF

MASTER OF SCIENCE IN ENGINEERING

BY

JIN-SEOK PARK

FEBRUARY 2021

Development of land cover classification model using CNN based FusionNet network and parcel boundary extraction algorithm

CNN기반의 FusionNet 신경망과 농지 경계추출 알고리즘을 이용한 토지피복분류모델 개발

지도교수 송 인 홍

이 논문을 공학석사 학위논문으로 제출함

2021년 2월

서울대학교 대학원

생태조경·지역시스템공학부 지역시스템공학전공

박 진 석

박 진 석의 공학석사 학위논문을 인준함

2021년 2월

위 원 장 (인)

부위원장 (인)

위 원 (인)

Abstract

The rapid update of land cover maps is necessary because spatial information of land cover is widely used in various areas. However, these maps have been released or updated in the interval of several years primarily owing to the manual digitizing method, which is time-consuming and labor-intensive. This study was aimed to develop a land cover classification model using the concept of a convolutional neural network (CNN) that classifies land cover labels from high-resolution remote sensing (HRRS) images and to increase the classification accuracy in agricultural areas using the parcel boundary extraction algorithm. The developed model comprises three modules, namely the pre-processing, land cover classification, and post-processing modules. The pre-processing module diversifies the perspective of the HRRS images by separating images with 75% overlaps to reduce the misclassification that can occur in a single image. The land cover classification module was designed based on the FusionNet model structure, and the optimal land cover type was assigned for each pixel of the separated HRRS images. The post-processing module determines the ultimate land cover types for each pixel unit by summing up the several-perspective classification results

and aggregating the pixel-classification result for the parcel-boundary unit in agricultural areas. The developed model was trained with land cover maps and orthographic images (area: 547 km^2) from the Jeonnam province in Korea. Model validation was conducted with two spatially and temporally different sites including Subuk-myeon of Jeonnam province in 2018 and Daseo-myeon of Chungbuk province in 2016. In the respective validation sites, the model's overall accuracies were 0.81 and 0.71, and kappa coefficients were 0.75 and 0.64, implying substantial model performance. The model performance was particularly better when considering parcel boundaries in agricultural areas, exhibiting an overall accuracy of 0.89 and kappa coefficient 0.81 (almost perfect). It was concluded that the developed model may help perform rapid and accurate land cover updates especially for agricultural areas.

Keywords: Land cover map, Land cover classification, Convolutional neural network, Parcel boundary

Student Number: 2019-26400

Contents

List of Figures

List of Tables

Chapter 1. Introduction

1.1. Study background

The way of land use is rapidly changing through the processes of adapting weather changes and civilization. Various aspects, including human behavior and ecosystem, are largely affected by the changed land use(Blasi et al., 2008; Yang et al., 2014; He et al., 2015). Land cover map, which implements the land use including spatial information, is an essential data to simulate the phenomenon. Real-time land cover map, especially on agricultural areas where land use could be changed every year, is necessary to track the land cover changes and suggest the future plan(Anderson et al., 2012; Schilling et al., 2008; Rahman, 2010; Bontemps, 2015; Borrelli, 2017).

Land cover maps, initially, were produced by the on-screen digitizing method, wherein a person reads the remote sensing image and classifies the land-use status. The Korea Ministry of Environment classifies land cover into 41 classes and provides land cover map using on-screen digitizing method. However, only limited area is turned into land cover maps per year, due to time consuming classification process(Laha et al., 2006; Shin et al., 2015).

Advancements in remote sensing technology enable us to obtain high resolution remote sensing (HRRS) images of an extensive area in short interval. Acquired HRRS images increase the potential to be used as basic data for creating a real-time land cover map (Enderle and Weih, 2005). Several land cover classification studies had been conducted for producing accurate and immediate land cover maps using HRRS images.

The pixel based methods were applied to classify land cover rapidly and accurately from remote sensing images, including several mathematical algorithms (Sakong, 2003; Enderle and Weih, 2005; Laha et al., 2006), artificial neural network (ANN) (Kang et al., 2006; Kang et al., 2012; Roy et al., 2015; Prasad et al., 2011; Huang and Zhang, 2012), and convolutional neural network (CNN) (Kussul et al., 2017; Fu et al., 2017; Lu et al., 2017; Carranza-García et al., 2019; Pan et al., 2020). A series of comparative studies confirmed that using CNN to classify the land cover showed better results than previous mathematical algorithms and ANN methods. The CNN accuracy showed 3-11% better than mathematical algorithms (Luus et al., 2015; Santoni et al., 2015), 1-4% better than SVM (Chen et al., 2014; Lee et al., 2015; Grinblat et al., 2016), and 2-41% better than MLP (Lee et al., 2015; Kussul et al., 2017). However, most of the previous CNN application studies have been conducted in relatively smaller

spatial areas with smaller numbers of land cover classes (Kussul et al., 2017; Fu et al., 2017; Lu et al., 2017; Carranza-García et al., 2019; Pan et al., 2020). So, land classifications were mostly made based on a single perspective image, which could be biased when application areas become larger.

Additionally, pixel based methods generate the optimal land cover label per pixel, and it could occur salt-and-pepper misclassification which isolated misclassified pixels existed on the correctly classified area (Darius and Justin, 2017). Object based land cover classification, which detects objects using a scale, color, shape, smoothness, and compactness and applies pixel based classification by a detected object, was conducted (Lee et al., 2011; Kim and Yeom et al., 2012). The aggregation of land cover classification results from pixels to boundary unit has the advantage to reduce the bias for classification. However, detected objects were different from real land use boundaries such as parcels and buildings. Therefore, it is necessary to devise a boundary extraction method suitable for each land cover, and to combine the extracted boundary with pixel based methods.

1.2. Objective of thesis

The objectives of this study were to develop a land cover classification model using the CNN concept under FusionNet structure and increase the accuracy of the developed model in agricultural areas by applying parcel boundary extraction algorithm.

The manuscript is divided into three chapters. Chapter 2 includes a literature review, which provides the basis for the thesis and indicates the direction of developing land cover classification model.

Chapter 3 described the methodology of land cover classification model development. Three main modules were established and combined including perspective diversification module for the pre-processing module, classifying land cover from orthographic image for CNN based land cover classification module, and aggregating land cover results in pixel to parcel unit for post-processing module.

Chapter 4 validate the accuracy of the developed model by applying it to different regions in terms of time and regions. Model validation was discussed with 41 child subcategories, 7 main categories, and 4 agricultural subcategories.

The FusionNet based land cover classification model development is quoted from development of land cover classification model using AI based FusionNet network (Park

et al., 2020). It was mentioned as footnotes that the cited portions were quoted at the beginning of each chapter.

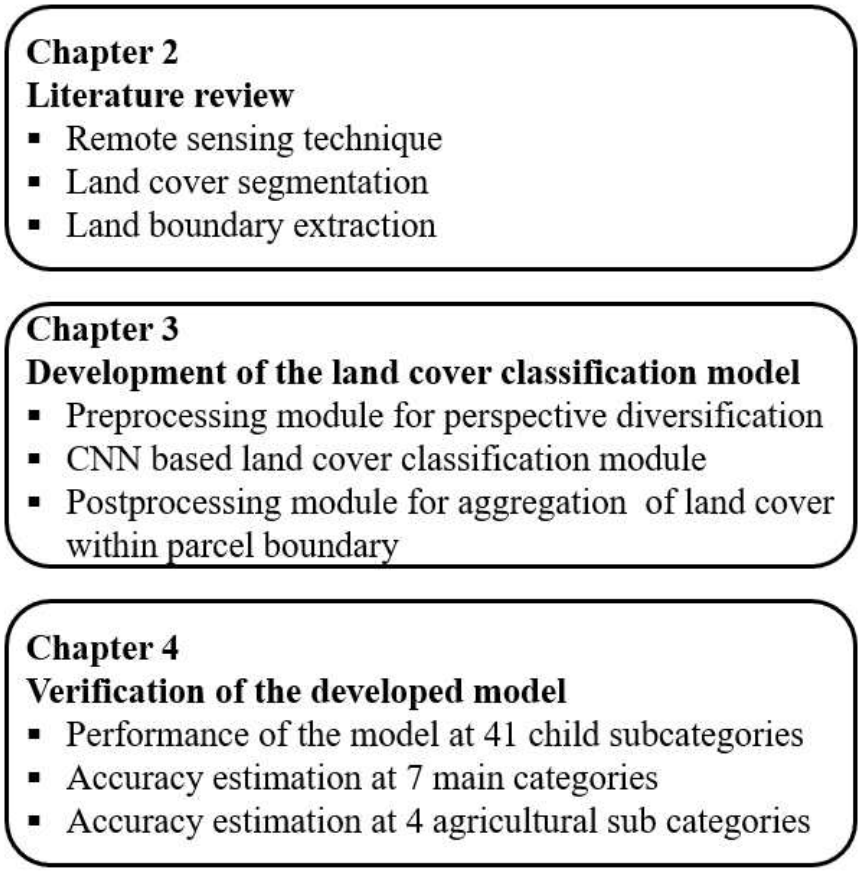

Figure 1-1 Flow diagram of this study

Chapter 2. Literature review

2.1. Development of remote sensing technique

Remote sensing techniques are the essential data for the study field which investigating the vast amount of area is needed, such as human behavior, ecosystem, climate, and also agricultural studies (Blasi et al., 2008; Yang et al., 2014; He et al., 2015; Anderson et al., 2012; Schilling et al., 2008; Rahman et al., 2010; Bontemps et al., 2015; Borrelli et al., 2017). The image obtained from remote sensing techniques is useful in that extract necessary information could be extracted according to the purpose of the usage, and the extracted information could be handled using geographic information system (GIS). Several platforms including satellite, airplane, and unmanned aerial vehicle (UAV) exist to obtain remote sensing data set with the development of remote sensing techniques.

Satellite image platform enables us to acquire a wide range of spatial coverage data with various observed wavelengths including red (R), green (G), blue (B), and near-infrared (NIR) bands. The time interval of remote sensing data provided from the satellite image platform is caused by the phenomenon of the satellite orbiting the earth. Satellite

image, mostly, has a lower resolution than other platform and the quality of the images could be affected by environmental factors such as clouds.

The representative satellite platforms are Landsat-8, Ikonos, Kompsat, and the provided resolution for RGB is 30m, 4m, 2.2m, and the recording interval is 16 days, 3 days, 1.4 days, respectively. Several studies were conducted to extracting useful information from satellite platforms. Examples of studies could be divided into four categories; human behavior (Kim et al., 2006; Oh et al., 2008); ecosystem (Cho and Oh, 2004; Choi and Kang, 2010; Choi et al., 2015); climate change (Park and Lee, 2017; Park et al., 2018); agricultural (Yeom and Kim, 2014)

The aerial platform provides aerial photographed images and orthographic images in which additional geometric corrections are conducted. The orthographic image has higher resolution and precision than satellite image through the use of observing camera and efforts of mapping research. But it has a limitation of long acquisition interval from the cost of precise aerial photography (Cho et al., 2014). The Korean National Geographic Information Institute (NGII) provide aerial photographs and orthographic images in the resolution of 0.51m with RGB and 2-year interval.

The main reason for starting aerial photography was surveying and creating a precise map from aerial

photographed maps conducted by several studies. Rabiu and Waziri (2014) produced orthographic images using ERDAS LPS software. And Kim and Um (2015) transformed aerial images into digital surface model (DSM) and orthographic images.

UAV platform, the latest methods, offer high resolution (less than 5cm) and near real-time image with less expense than satellite and aerial platforms. UAV photograph with a general camera, not the precise observation camera, and generate corrected images using the overlapped points (Barazzetti et al., 2014; Yoo et al., 2016).

UAV platform, capable of acquiring real-time information from the characteristics of simple photograph and image processing, is being used for several studies including disaster management (Roy et al., 2015; Prasad et al., 2011; Huang and Zhang, 2012), surveying and mapping (Kang et al., 2006; Kang et al., 2012; Schöpfer et al., Areas 2010; Längkvist et al., 2016; Kamilaris and Prenafeta, 2018; Gavade and Rajpurohit, 2019) agriculture and forest change detection (Sakong and Im., 2003; Enderle and Weih, 2005; Laha et al., 2006; Jin et al., 2019; Paisitkriangkrai et al., 2016), and crop production (Na et al., 2019).

2.2. Land cover segmentation[1)]

Development of remote sensing technology provide high resolution images, which implies vast amount of information. Several efforts to extract desired information for each study fields are being made. Land cover classification field is necessary to provide precise map, which was the original purpose of remote sensing technology, in that it could be served as basic data for all studies.

In the early stages of land cover classification, the on-screen digitizing method was used, in which person identified each land cover by reading the orthographic images and referencing the already possessed map including the clinical map, cadastral map etc. Korean Ministry of Environment began providing main-category land cover map with 7 categories in the 1980s using on-screen digitizing method. KME has been providing it as sub-category with 22 items and child-category with 41 items, according to the development of HRRS imagery and the need for detailed land use information. As information becomes more sophisticated and categories increased, on-screen digitizing method has limitation of time consuming and labor intensive to create real time land cover map.

---

1) Chapter 2.2. is quoted from development of land cover classification model using AI based FusionNet network (Park et al., 2020).

Several studies, utilizing various methods to produce accurate and immediate land cover map, were conducted including mathematical algorithms and ANN concept methods. In the application of mathematical algorithms, multifarious algorithms such as parametric method, maximum likelihood method, fuzzy theory, supervised classification were used to classify the land use. Sakong (2003) compared results of visual reading with results of parameter method, fuzzy theory, non-supervised classification algorithms, for land cover classification through videos. Enderle (2005) classified the land cover by combining the supervised and unsupervised classification methods, while Laha (2006) used the fuzzy theory to classify the land cover. However, with the advancement of the remote sensing technology, it became possible to obtain a high-resolution remote sensing (HRRS) image which widened a spectrum of a single land-use cases (Jin, 2019). This has resulted in reducing the effects of the previous land cover classification method (Paisitkriangkrai, 2016).

ANN concept based studies such as SVM, MLP and CNN were conducted to classify land covers accurately from HRRS image with a larger amount of information. Several studies conducted using prototype of ANN concept including SVM and MLP. Kang (2006) used the maximum likelihood method and MLP to classify the land cover and it was confirmed that

the land cover classification was more accurate in MLP. Kang (2012) compared the results through the maximum likelihood method, artificial neural network, and SVM while Moumita Roy (2015) compared the results through k-nearest neighbor technique (KNN), MLP, and SVM. A series of comparative studies confirmed that using the prototype of ANN to classify the land cover produced better performance compared with using the mathematical algorithm. However, prototype of ANN based land cover classification has limitation that it is difficult to considering the spatial distribution of images according to the properties of trained with sing DN of a single pixel.

CNN, the developed form of ANN, was developed to considering the difficulty and has been applied to image classification (Längkvist et al. 2016). The accuracy of CNN model is affected by the CNN structures and the quality of the training data set (Jin et al., 2019; Kamilaris and Prenafeta, 2018; Gavade and Rajpurohit, 2019). For an optimal structure, trial-and-error method is needed, and several studies tried to develop optimal structure by combining basic components of CNN. Developed different CNN structure increased the classification accuracy compared to Mathematical algorithms. The CNN accuracy showed 3-11% better than mathematical algorithms (Luus et al., 2015; Santoni et al., 2015), 1-4% better than SVM (Chen

et al., 2014; Lee et al., 2015; Grinblat et al., 2016), and 2-41% better than MLP (Lee et al., 2015; Kussul et al., 2017).

Several CNN models are applied on land cover classification, which segments land use per each pixel of the entire image, using different training data sets. Nataliia Kussul classified major summer crop types to 11 categories using Landsat-8 and Sentilel-1A image (Kussul et al., 2017). Gang Fu trained model to 12 categories of urbanized area with GF-2 image and tested on several 1 km2 area using other GF-2 and IKONOS satellite image (Fu et al., 2017). LU Heng distinguished cultivated land from whole image of 0.5 km2 obtained from unmanned aerial vehicle (Lu et al., 2017). Manuel Carranza-García used AVIRIS and ROSIS image to train 16 classes of crops in agricultural area and AirSAR for training urbanized area with 12 classes and verified 6.5 km2 of agricultural area and 5.0 km2 of urbanized area (Carranza-García et al., 2019). Suoyan Pan classified 3.2 km2 of land cover to seven categories using multi-spectral LiDAR (Pan et al., 2020). However, most of the previous studies have been conducted in relatively smaller spatial areas with smaller numbers of land cover classes.

2.3. Land boundary extraction

Real-time land cover map of agricultural area is important data for Geographical Information Systems (GIS) to tracking the land use change, estimating production and providing appropriate financial support from nation. Conversion of land cover map from HRRS image requires not only segmented land cover information, but also accurate parcel boundary extraction. Several studies have been conducted to extract field parcel boundaries, grouped with 3 categories; edge-based methods; region-based methods; and ANN-based methods.

Edge-based methods use filters to extract the parcel edge from detecting abrupt gradient change. Mustafa Turker and Emre Hamit Kok (2013) extracted sub-field boundary from satellite imagery using canny edge detection and simplicating the line with Douglas-Peucker algorithm. L. Yan and D.P. Roy (2014) divided crop field and non-fields from landsat imagery using the distance from WELD reference data and watershed algorithm to refine the extracted boundary. Edge-based methods, however, have a limitation that extracted field boundary could be more simplified or sensitive than reality depending on the filters.

Region-based methods separate the specific land cover using textural properties of each land use from the

adjustment of threshold parameter. Segl, Karl and Hermann Kaufmann (2001) distinguished small objects like building and vegetation fields from HRRS images by modifying the threshold. And Mulleller et al. (2004) developed extracting liner boundary by upgrading previous Segl, Karl and Hermann Kaufmann (2001) study. Da Costa et al. (2007) extracted vine parcels from HRRS images based on the textural properties. Yet, region-based methods have drawbacks in that the extracted boundaries are highly dependent on parameter selections.

ANN-based methods are in progress to produce accurate field boundaries using ANN architecture and training with already classified field boundary data. A. García-Pedrero et al. (2016) delineation the agricultural parcel using the machine learning approach. And Waldner, François, and Foivos I. Diakogiannis (2020) extracting field boundaries from satellite images using CNN architecture.

Chapter 3. Development of land cover classification model[2)]

3.1. Conceptual structure of the land cover classification model

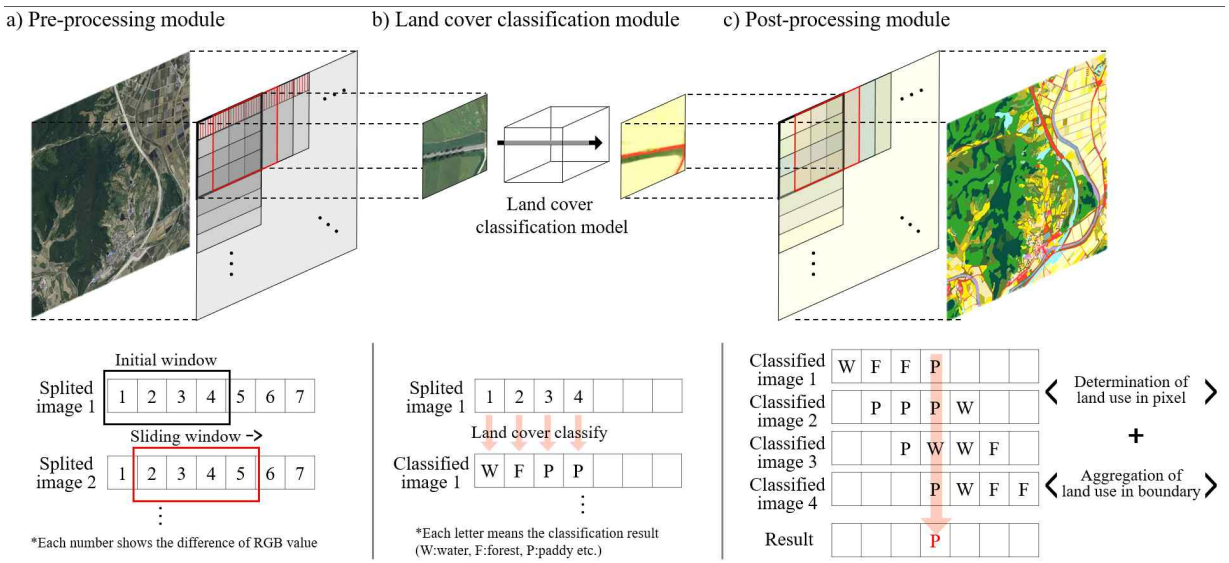

Figure 3-1 Flow chart of the land cover classification model (modified from Park et al., 2020)

2) Chapter 3.1. to 3.3. are quoted from development of land cover classification model using AI based FusionNet network (Park et al., 2020).

3.2. Pre-processing module

The CNN based land cover classification classify the land cover label from HRRS image considering the spatial distributions of color values of each pixel, not simply allocate land uses by color values of pixels. Land cover classification using only a single HRRS image, depending on the view point, could lead to biased land cover classification result. The pre-processing module was applied to diversify the perspectives of HRRS images.

Pre-processing module separate the orthographic image into unit image with overlapping to diversification of perspectives. The size of unit image was set to 256 x 256 pixels (about 130m x 130m) considering the size of artificial land use and computer performance. Each image was 75% (shifting 64 pixels) overlapped both in the horizontal and vertical directions (Figure 3-2). Finally, 16 images with different perspectives were used to classify land uses in a single space (Figure 3-2 Red hatched area).

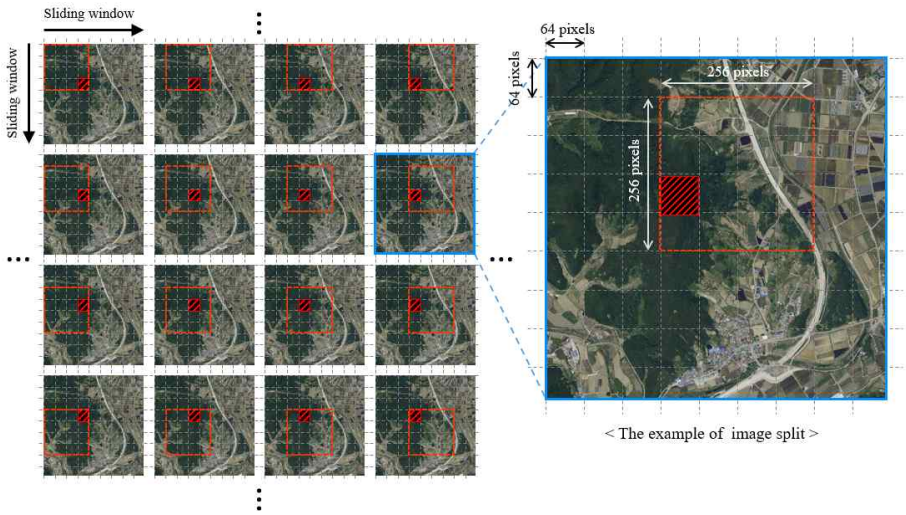

Figure 3-2 The process of pre-processing module (Land cover information of Red hatched area could be extracted from 16 different viewpoint.) (Park et al., 2020)

3.3. CNN based land cover classification module

The land cover classification module converts the input image into a land cover map, in which the land use status is segmented semantically by respective land cover color codes (please refer to Table 4-1). CNN was used for an effective image segmentation of the land cover, and FusionNet (Quan et al., 2016) of CNN, which separates cell from EM image (Ronneberger et al., 2015; Çiçek et al., 2016) was conceptually similar to the creating land cover maps that identifies land use boundary using HRRS image, was used as the structure of the neural network.

The entire land cover classification module largely consists of two processes: encoding (Figure 3-3 (a)) that classifies land use features from the image data, and decoding (Figure 3-3 (b)) that prints the land use map classified through different colors according to the classified land use features. The module is configured with a combination of four basic layers of the convolutional layer, residual layer, down-sampling and up-sampling, and summation-based skip connection.

As a layer that is widely used in the deep learning field, the convolutional layer converts the entered data into compressed data including special information in the processes of convolution, activation function, and batch normalization (Shang et al., 2016). Parameters used in the configuration of convolutional layer in this module are kernel size of 3, stride of 1, and padding of 1. In general, the rectified linear unit (ReLU) is used in the activation function (Equation (1)). However, in ReLU, the gradient value always becomes negative if the entered value is negative. Data compression using ReLU in the encoding process could result in data losses. Leaky ReLU, which can provide gradient value when the input value is negative, can complement ReLU (Equation (2)). Therefore, the module was configured with Leaky ReLU as an activation function in the encoding process and ReLU as an activation function in the decoding

process.

$$ReLU : f(x) = \max(0, x) \quad (1)$$
$$leaky\,ReLU : f(x) = \max(0.01x, x) \quad (2)$$

The residual layer is configured with three convolutional layers and a single summation-based skip connection. The neural network deepens, and the data features become noticeable through the three convolutional layers included in the residual layer. However, as the neural network deepens, a gradient vanishing problem occurs. To solve this issue, we used the summation-based skip connection in the residual layer, which integrates the past data with the currently processing data in the module, and configured the layer to enable a more exquisite classification (Quan et al., 2016).

Down-sampling was used to reduce computation volume and prevent overfitting (Zeiler and Fergus, 2013). Maxpooling function that brings the largest value within each stride was also used. In the down-sampling process, a kernel size of 2, stride of 2, and zero padding were used. In contrast to the down-sampling, the up-sampling increases the layer size to acquire images segmented by colors from the land use classification results. The deconvolution function was used for up-sampling.

Summation-based skip connections, which solve the gradient vanishing issue and help the information transfer, were used in the residual layer and long skip connections.

So, the convolutional layer could be much deeper to include more parameters without losing its training efficiency. Skip connections function to merge the previous layer and the current layer by summing the matrix of each layer. Short skip connections in residual layer add up first convolutional layer with third convolutional layer. Four long skip connections connect the layer of the encoding path to the decoding path, which are the same size.

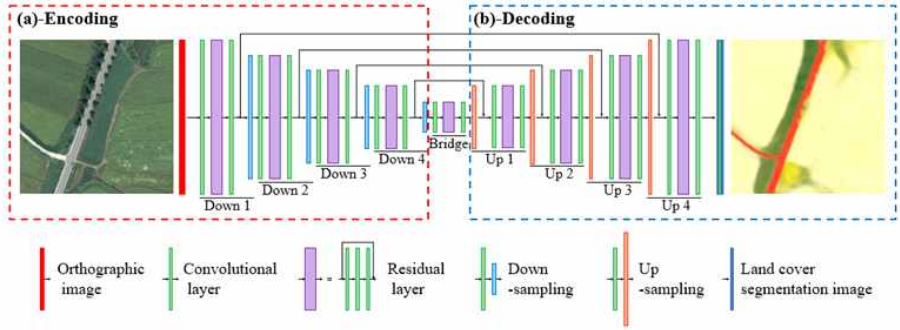

Type		Layer Structure	Size of layer
Input			256 × 256 × 3
Encoding	Down 1	Convolutional + Residual + Convolutional + max pooling	256 × 256 × 64 128 × 128 × 64
	Down 2	Convolutional + Residual + Convolutional + max pooling	128 × 128 × 128 64 × 64 × 128
	Down 3	Convolutional + Residual + Convolutional + max pooling	64 × 64 × 256 32 × 32 × 256
	Down 4	Convolutional + Residual + Convolutional + max pooling	32 × 32 × 512 16 × 16 × 512
Bridge		Convolutional + Residual + Convolutional	16 × 16 × 1024
Decoding	UP 1	Deconvolutional + Merge + Convolutional + Residual + Convolutional	32 × 32 × 512 32 × 32 × 512
	UP 2	Deconvolutional + Merge + Convolutional + Residual + Convolutional	64 × 64 × 256 64 × 64 × 256
	UP 3	Deconvolutional + Merge + Convolutional + Residual + Convolutional	128 × 128 × 128 128 × 128 × 128
	UP 4	Deconvolutional + Merge + Convolutional + Residual + Convolutional	256 × 256 × 64 256 × 256 × 64
Output		Convolutional	256 × 256 × 3

Figure 3-3 Architecture of the convolutional neural network (CNN) based land cover classification module (Park et al., 2020).

3.4. Post processing module

3.4.1 Determination of land cover in a pixel unit[3)]

The primary function of determination of land use in pixel unit integrates module is to analyze and integrate classified images of 16 different perspectives, produced from the pre-processing and the land cover classification modules, into a final land cover using numerical and statistical methods. The module of determination of land use in pixel unit consists of two parts of land cover assignment to a pixel level and following land cover integration to determine the final land cover to a given pixel.

Land cover assignment part is the process to determine land cover to a pixel based on the classified output. The R, G, B values of classified image pixels are the output by the classification model that were trained with land cover map color (label). The model output values do not match exactly to the reference values of land cover map since the trained CNN works only to minimize errors. The Gaussian distance was used to find nearest land cover to a given pixel by calculating the distance between the classified color values (result) with reference land cover code (label). The formula

3) Chapter 3.4.1. is quoted from development of land cover classification model using AI based FusionNet network (Park et al., 2020).

to calculate Gaussian distance is given in Equation (3). The label land cover with the lowest Gaussian distance was assigned to a given pixel.

$$Gaussian Distance = \sqrt{(R_{result} - R_{label})^2 + (G_{result} - G_{label})^2 + (B_{result} - B_{label})^2} \quad (3)$$

where each R_{result}, G_{result}, and B_{result} means red, green, blue values represent output produced by the land cover classification module. R_{label}, G_{label}, B_{label} means red, green, blue values indicate the reference values specific to each sub-category of land cover maps given in Table 4-1. The reference color code is standardized and provided by the Korean government.

The land cover integration is a process of aggregating the land cover classification results that are classified through images of 16 different perspectives of one region, to determine the final land cover classification result. The 16 different classification results per pixel that were obtained from the pre-processing, the land cover classification module, and the pixel land use determination process of the determination of land use module were aggregated to produce the final result. The item selected as having the greatest number of land cover classification results among the aggregated land cover classification items was determined as the final land use classification result (Equation (4). When the maximum counts are same for the different land covers,

then one of them was chosen arbitrarily. The final land use classification result per pixel is printed as a final land cover classification map in which the classification of the aggregated orthographic image input is complete.

$$Classification\,Result = \max(count_{paddy}, count_{water}, count_{forest}, etc \quad (4)$$

where $count_{item}$ is the number of the classified item out of the total classification results.

3.4.2 Aggregation of land cover to parcel boundary

The CNN based land cover classification module produces the optimal land cover classification per pixel, not per parcel with boundaries. In reality, however, agricultural areas are used in the form of parcels with boundaries. Aggregation of land cover to parcel boundary module is applied to produce a land cover map that is similar to the actual land use.

The main function of aggregation of land cover to parcel boundary module is extracting the boundary of agricultural area, regardless of the crop type or cultivation type, and assigning the most land use in pixel unit, from the determination of land use module, as land cover in parcel boundary. Aggregation of land cover to parcel boundary module is composed up of three part including external edges detection, internal edges detection, and aggregation of

pixel based land cover to boundary based.

External edge detection, which is the region-based methods, distinguish the agricultural region from the others by detecting the abrupt gradient difference. External edges detection is composed of gray scaling and application of three main algorithms including Otsu's algorithm, Suzuki85 algorithm and Ramer-Douglas- Peuker algorithm.

Orthographic images including R, G, B were converted into gray scaled with one representative value (Equation (5) and Figure 3-4 (a)) for image generalization (Lakhwani et al., 2015).

$$\mu = 0.299R + 0.587G + 0.114B \quad (5)$$

Where, μ represents gray scaled value and each R, G, and B means red, green, and blue, respectively.

Gray scaled image is binarized with estimated threshold from Otsu's algorithm (Equation (6) and Figure 3-4 (b)), which determine the threshold minimizing the variance from pixels (Otsu, 1979). This process could solve the problem of region-based method, in which the accuracy is affected depending on the threshold, and made it applicable regardless of the image.

$$BI_{xy} = \begin{cases} 0 & ;\mu_{xy} < T \\ 255 & ;\mu_{xy} \geq T \end{cases} \quad (6)$$

Where, BI_{xy} represents the binarized value, μ is gray scaled image value, and T means threshold obtained from Otsu's

algorithm.

Image contours are extracted from binarized image using Suzuki85 algorithm (Figure 3-4 (c)), which construct contours by setting a starting point and searching boundaries in clockwise and counterclockwise from adjacent points (Suzuki & Abe, 1985; Lee et al., 2016).

Extracted contours are then simplified into polygons representing agricultural region by applying the Ramer-Douglas-Peuker algorithm, which defines dissimilar points as vertex and removes other similar points based on the distance from line and points (Figure 3-4 (d)). In this study, the maximum distance was set to approximately 0.0001.

Internal edges detection, which is edge-based method, was applied to extract sensitive edge such as the boundary between parcels and other parcels. Internal edges are separated within the extracted external edges by following four steps including gray scaling, Canny edge detection, Hough transform and ray casting algorithm, and noise canceling process.

Gray scaling is adapted to image generalization, same as the extracting external edges (Equation (5) and Figure 3-4 (e)). And edges are extracted in binary image form using Canny edge detector, image filter specialized in detecting edge (Figure 3-4 (f)). Several processes are conducted to

detect the edges (Canny, 1986); Gaussian smoothing to reduce the noise using Gaussian filter (Hagen & Dereniak, 2008); Gradient filtering to select the preliminary edges which have high spatial derivatives; Non-maximum suppression to eliminate the pixel that is not at the maximum; Hysteresis thresholding to extract specific edges which satisfying two thresholds of objective. In this study, 3x3 sized Sobel kernel was applied to the Gaussian smoothing and thresholds for parcel boundaries were set to 80 and 240.

Hough transform and ray casting algorithm were applied to handle the problem of the edge-based methods that the divided boundary could be more simplified or sensitive than reality depending on the filters. Edges extracted from Canny edge detection include various length and uncertain values hindering the accurate internal edge detection. Using Hough transform, all edges in X and Y plane were transformed with r and theta plane to express the various lines and find the intersections (Richard & Peter, 1971). And some edges are ignored that the edges with a length are less than 25 pixels and the distance between edges are within 3 pixels. While edges with more than 60 intersections are selected as valid edge. Selected valid edges are expanded to extracted outer boundaries using ray casting algorithm (Figure 3-4 (g)), which could determine the nearest outer boundaries (Shimrat, 1962).

Noise canceling processes are conducted by removing the dense lines, and by eliminating the lines with unusual angles (Figure 3-4 (h)).

As the final process of aggregation of land cover to parcel boundary module, aggregation of pixel (Figure 3-4 (B)) to boundary based land cover to boundary based (Figure 3-4 (C)) is conducted. In each parcel boundaries, land cover categories are counted and the most counted categories are synthesized as the land use of the boundary (Figure 3-4 (C)).

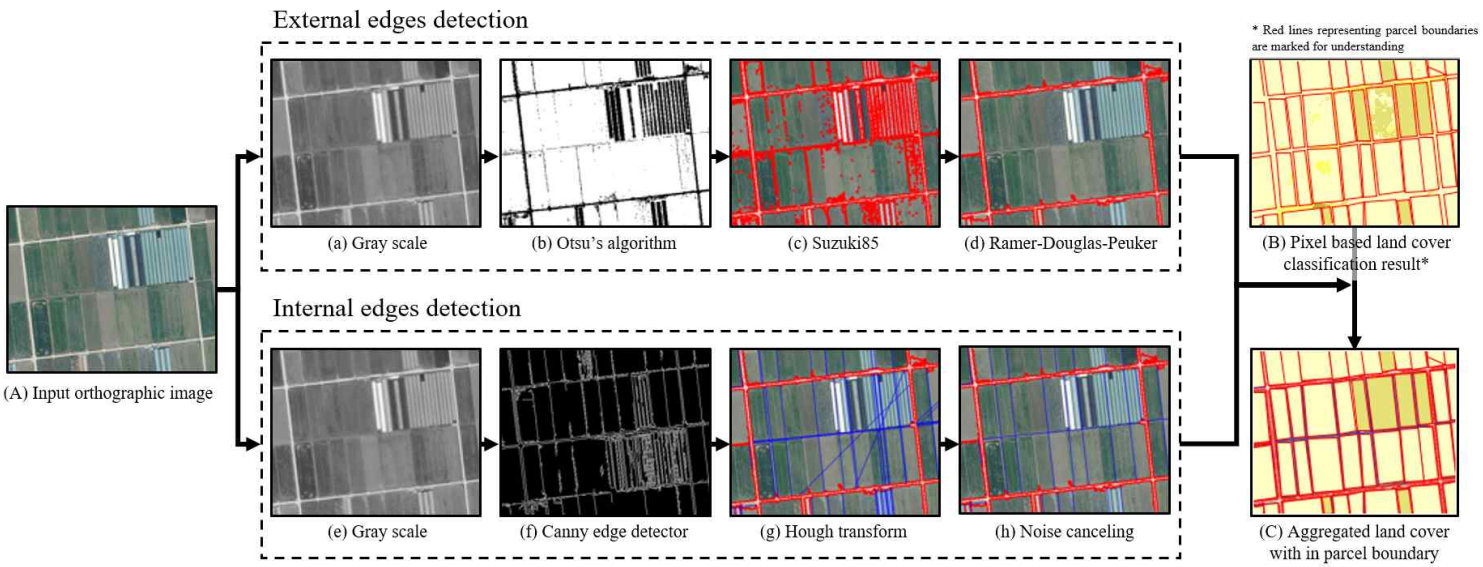

Figure 3-4 The whole process of aggregation of land cover to parcel boundary

Chapter 4. Verification of the land cover classification model[4)]

The schematics of the developed model training and verification is shown in Figure 4-1. Developed model was trained and validated with two different regions in terms of time and regions. And verification results were discussed with 41 child subcategories, 7 main categories, and 4 agricultural subcategories.

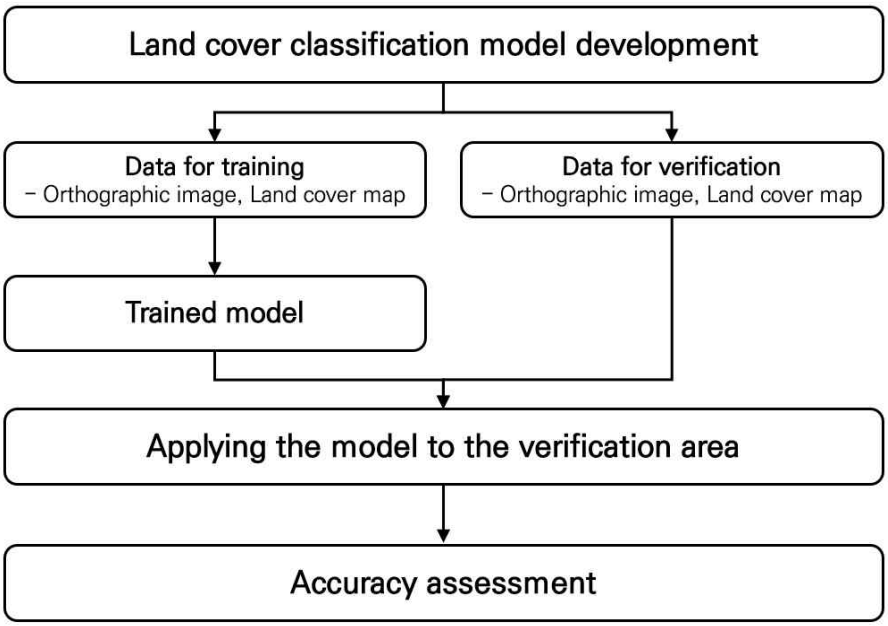

Figure 4-1 Schematics of the study procedure (Park et al., 2020)

4) Chapter 4.1. and 4.2. are quoted from development of land cover classification model using AI based FusionNet network (Park et al., 2020).

4.1. Study area and data acquisition

4.1.1. Training area

To train the land cover classification model, a training area of 547.3 km^2 was selected, which could acquire the latest source data of 2018 and contain the largest cultivating area in South Korea. The selected area included a cultivated acreage of 22,495 ha in Yeongam-gun and 20,279 ha in Muan-gun, and is a useful area for training the model for agricultural land cover (KOSTAT, 2020). In addition, it could also train the model for urban land cover, as it includes the main urban areas, such as the Gun offices in Jeonnam province, Mokpo City Hall, etc., which are some of the major buildings in the urban center. The areas selected for the study are shown in Figure 4-2.

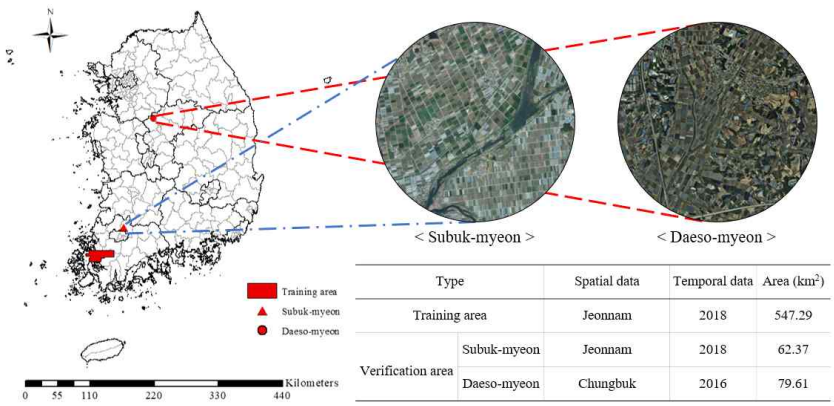

Type		Spatial data	Temporal data	Area (km^2)
Training area		Jeonnam	2018	547.29
Verification area	Subuk-myeon	Jeonnam	2018	62.37
	Daeso-myeon	Chungbuk	2016	79.61

Figure 4-2 Study area of training and verification (Park et al., 2020)

4.1.2. Verification area

The artificial intelligence (AI) based land cover classification is likely to be the most accurate for data that have spatial and temporal dimensions similar to that of the training data. To increase the accuracy of model verification, this study selected two separate areas for the verification process; one area had spatial and temporal dimensions similar to that of the training area and the other area was located far from the training area and had different time periods.

An area of 62.4 km^2 in Subuk-myeon, Jeonnam province, in 2018 was selected as the first verification area. For the Subuk-myeon area, an orthographic image source data obtained for the same period as that of the study data (2018) exists, and spatially, it is located in the same region as the study data (Jeonnam province).

As the second verification area, an area of 79.61 km^2 in Daeso-myeon, Chungbuk province, in 2016 was selected. Daeso-myeon was selected because an orthographic image source data recorded at a different time period (2016) and located far from the study data was available. These two verification areas are shown in Figure 4-2.

4.1.3. Data acquisition

A. Orthographic image

The orthographic images of the study area (2018) and the verification areas (2018, 2016) were obtained from the National Geographic Information Institute (NGII). The orthographic images are produced through geometric correction and orthometric correction of aerial photographs recorded in each period. The spectral channels of HRRS image include the red, green, and blue bands. The resolution of the orthographic images of the established study area (2018) and verification areas (2018, 2016) is 51 cm/pixel.

B. Land cover map

The land cover maps of the selected sites for model training (2018) and the two verification sites (2018, 2016) were established using the Korean Environmental Geographic Information System (EGIS). The land cover maps of EGIS are the results of on-screen digitizing of the orthographic images from the NGII by assigning various colors to respective land use types as shown in Table 4-1. It should be noted that the color codes were thoughtfully assigned that the sub-category-classes under a main category have similar color hues, i.e., red for urbanized area, yellow for

agricultural land, dark green for forest, light green for grassland, violet for wetland, light blue for barren lands, and dark blue for water. The land cover map was used as the ground truth serving as the target for the supervised model training. As previously described in Equations (3) and (4), the color codes in Table 4-1 were also used for calculating the Gaussian distance for the land cover assignment to the pixel level. The land cover map is presented in three different categories based on the level of detail; seven items in the main category, 22 items in the parent subcategory, and 41 items in the child subcategory.

C. Farm map

The farm map, which was specialized in agricultural area, were obtained from Korean public data portal. It provides agricultural land cover with parent subcategory in parcel boundary unit. Provided farm map has delay in update due to the methods of manually extracting boundaries from orthographic image. So, a farm map that most temporally matched with orthographic images were used as ground truth of parcel boundary. Established temporal year of orthographic image and farm map was 2018 and 2017 in Subuk-myeon, respectively. And the same 2016 orthographic image and farm map was used in Daeso-myeon.

Table 4-1 Hierarchy of land cover categories and respective color codes (Environmental Geographic Information System (EGIS)).

Main Category (7 items)	Parent Subcategory (22 items)	Child Subcategory (41 items)	Color Code			
			R	G	B	Remark
Urbanized area	Residential area	Single housings	254	230	194	
		Apartment housings	223	193	111	
	Industrial area	Industrial facilities	192	132	132	
	Commercial area	Commercial and office buildings	237	131	184	
		Mixed use areas	223	176	164	
	Culture and sports recreation area	Culture and sports recreation facilities	246	113	138	
	Transportation area	Airports	229	38	254	
		Ports	197	50	81	
		Railroads	252	4	78	
		Roads	247	65	42	
		Other transportation and communication facilities	115	0	0	
	Public facilities area	Basic environmental facilities	246	177	18	
		Educational and administrative facilities	255	122	0	
		Other public facilities	199	88	27	
Agricultural area	Paddy	Consolidated paddy filed	255	255	191	
		Paddy field without consolidation	244	230	168	
	Upland	Consolidated upland	247	249	102	
		Upland without consolidation	245	228	10	
	Greenhouse	Green houses	223	220	115	
	Orchard	Orchards	184	177	44	
	Other cultivation lands	Ranches and fish farms	184	145	18	
		Other cultivation plots	170	100	0	
Forest	Deciduous forest	Deciduous forests	51	160	44	
	Coniferous forest	Coniferous forests	10	79	64	
	Mixed forests	Mixed forests	51	102	51	
Grassland	Natural grassland	Natural grasslands	161	213	148	
	Artificial grassland	Golf courses	128	228	90	
		Cemeteries	113	176	90	
		Other grasslands	96	126	51	
Wetland	Inland wetland	Inland wetlands	180	167	208	
	Coastal wetland	Tidal flats	153	116	153	
		Salterns	124	30	162	
Barren lands	Natural barren	Beaches	193	219	236	
		Riversides	171	197	202	
		Rocks and boulders	171	182	165	
	Artificial barrens	Mining sites	88	90	138	
		Sports fields	123	181	172	
		Other artificial barrens	159	242	255	
Water	Inland watery	Rivers	62	167	255	
		Lakes	93	109	255	
	Marine water	Marine water	23	57	255	

4.2. Training the land cover classification model

The location adjustment of the established orthographic images and land cover maps of the study area was made using ArcMap (ESRI, Ver. 10.1). To train the land cover classification model, acquired data were split vertically and horizontally with 256 × 256 pixels (130 m × 130 m), which is an appropriate size for confirming the land uses. The land cover map classified by colors of the child subcategory (41 items) was used for the model training. A total of 32,384 orthographic images and 32,384 land cover maps of the same area were created.

For effective model training, an image augmentation process that increases the number of the study data was performed. The level of the diversification of the study data was increased by rotating the generated orthographic images and land cover maps at angles of 0˚, 90˚, 180˚, and 270˚. Finally, 129,536 sheets of each orthographic image and land cover map were used for training the model.

The model training was conducted using Intel i7-9700K CPU and NVIDA GeForce GTX 1060 6gb hardware, and using the Python (Ver. 3.6.8) and PyTorch (Ver. 1.0.1) software. Mean square loss (MSELoss) was used for estimating errors in the model, and the training was completed when the error value was less than 0.01. The training was completed with MSELoss

value of 0.0077 after training 129,536 sheets of the established study data 84 times.

4.3. Verification method

4.3.1. The performance measurement methods of land cover classification model[5)]

The accuracy of the land cover classification was evaluated by creating accuracy metrics that indicated consistencies of items between the evaluation results of the two evaluators and by estimating the quantitative index values for overall accuracy and kappa coefficient based on the metrics.

The accuracy metrics were created by comparing the land cover classification map created by the on-screen digitizing method (reference land cover) with that created classified by the developed model (classified land cover). The consistent land cover classification results of both evaluators (reference land cover, classified land cover) were indicated on the diagonal matrix of accuracy metrics.

Producer's accuracy and user's accuracy show the ratio of correctly matched area of each land use in reference data and classified data, respectively (Equation (7) and (8)). The overall accuracy was estimated using Equation (9), which

5) Chapter 4.3.1. is quoted from development of land cover classification model using AI based FusionNet network(Park et al., 2020).

indicates the ratio of the correctly classified land cover area to the entire area. Three accuracy indicator has values ranging from 0 to 1, and the classification becomes more accurate as this value comes closer to 1. Although the overall accuracy enables an intuitive accuracy evaluation of the land cover classification, it has a limitation of not being able to consider a possibility of accidentally assigning the same land cover classification for different areas.

Thus, a kappa coefficient, which excluded the probability of accidental consistency in the overall accuracy, was also used in the accuracy evaluation of the land cover classification. The kappa coefficient means a value compared with a randomly arranged accuracy metrics (Equation (10)). The kappa coefficient has values ranging from -1 to 1, and as the value gets closer to 1, the classification attains a higher accuracy. Model performance was evaluated by the strength criteria(Table 4-3) provided by Landis and Koch (Landis and Koch, 1977).

Table 4-2. A example of accuracy metrics

		Classified Data				Producer's accuracy (%)
		Paddy	Water	Forest	Total	
Reference Data	Paddy	23	6	0	29	79.3
	Water	5	31	3	39	79.5
	Forest	7	3	22	32	68.8
	Total	35	40	25	100	-
User's accuracy (%)		65.7	77.5	88.0	-	-

$$\text{Producer's accuracy} = \frac{x_{ij}}{x_{i+}} \quad (7)$$

$$\text{User's accuracy} = \frac{x_{ij}}{x_{+j}} \quad (8)$$

$$\text{Overall accuracy} = \frac{\sum_{i=1}^{k_x} x_{ii}}{N} \quad (9)$$

$$\text{Kappa coefficient} = \frac{N \times \sum_{i=1}^{k} x_{ii} - \sum_{i=1}^{k} x_{i+} \times x_{+j}}{N^2 - \sum_{i=1}^{k} x_{i+} \times x_{+j}} \quad (10)$$

where, i and j represent each row and column, respectively, and N denotes total number of the classification result.

Table 4-3 Strength of agreement according to kappa coefficient value(Landis and Koch, 1977)

Kappa coefficient	Strength of Agreement
-1.0-0.0	Poor
0.0-0.2	Slight
0.2-0.4	Fair
0.4-0.6	Moderate
0.6-0.8	Substantial
0.8-1.0	Almost Perfect

4.3.2. Accuracy estimation methods of agricultural parcel boundary

Extracted agricultural parcel boundaries from Aggregation of land cover to parcel boundary module are not including

land cover information such as paddy, field, and greenhouse etc. It only implies whether it is the boundary of agricultural land or not. The accuracy of extracted agricultural parcel boundaries was evaluated using precision, recall.

The indicators of true positive (TP), false positive (FP), true negative (TN), and false negative (FN), which representing the agreement of predicted boundaries and ground truth, were first calculated (Table 4-4). Based on the assumption that predicted boundaries from model is positive, TP is evaluated if prediction matched (true) with ground truth and FP is evaluated if prediction mismatched (false) with ground truth. Precision, which indicates the predicted boundaries accuracy, were calculated from the accurate boundary (TP) overestimated accurate boundaries (TP + FP) (equation 11)).

Assuming that predicted boundaries from model is negative, TN and FN is estimated depending on whether predicted nonboundary (negative) was matched with ground truth (true, TN) or not (false, FN). Recall, demonstrate the accuracy of detecting boundary, was estimated based on equation 12.

In general, judgment of match or mismatch were estimated from threshold of coincidence ratio like intersection over union (IOU). In this study, judgment of match was performed based on pixel and the threshold which was set to 1.

Table 4-4 An example of precision and recall

Ground truth	Predicted results	
	Positive	Negative
Positive	TP (true positive)	FN (false negative)
Negative	FP (false positive)	TN (true negative)

$$\mathrm{Precision} = \frac{TP}{all\ \mathrm{detections}} = \frac{TP}{TP+FP} \tag{11}$$

$$Recall = \frac{TP}{all\ ground\ truths} = \frac{TP}{TP+FN} \tag{12}$$

4.3.3. Comparison of boundary based classification result with ERDAS Imagine

Pixel with boundary based classification model result, which was produced by combining pixel and parcel classification result, was verified using an objective workstation of commercial software ERDAS Imagine (HEXAGON, version 14).

The agricultural land cover classification from the objective workstation was performed through the following three processes. The orthographic image was simplified using the single feature probability (SFP) method, and 15 land cover information for each agricultural areas were inputted. And the agricultural land cover was extracted through the processes of probability filter 0.7, generalize, and smooth.

4.4. Verification of land cover classification model[6)]

4.4.1. Performance of land cover classification at the child subcategory

Model performance in land cover classification for the respective Subuk-myeon (Jeonnam province, 2018) and Daeso-myeon (Chungbuk province, 2016) was presented in terms of the number of classified land cover that matches with the reference land label as shown in Figure 4-3. A total of 41 land covers at the child subcategory level were classified with the developed model (Figure 4-3). As shown from the darker gray along the diagonal direction, the developed model performed reasonably well in land cover classification. Overall, the model demonstrated better accuracy for the urban, agriculture, forest and water areas, while relatively poor in grass, wetlands, and barren lands showing the wider spectrum of classified land covers.

6) Chapter 4.4.1. and 4.4.2. are quoted from development of land cover classification model using AI based FusionNet network (Park et al., 2020).

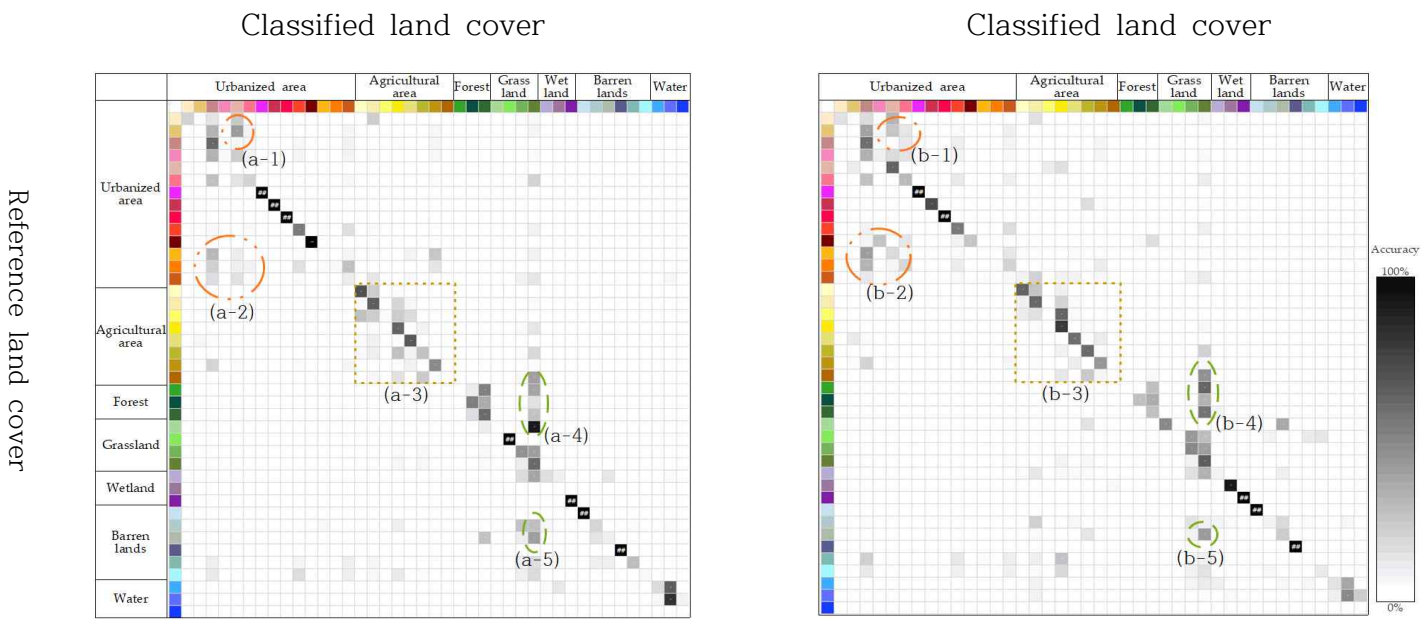

(a) Subuk-myeon (b) Daeso-myeon

Figure 4-3 Model performance matrices for (a) the Subuk-myeon and (b) Daeso-myeon areas. The accuracy was presented in gray scale based on the percentage of the classified pixels that batch with the reference land cover label to the total number of pixels. The darker gray indicates the more pixels were classified to the given land cover. Refer to the color codes for detailed land cover given Table 4-1 (Park et al., 2020).

Most of misclassifications at the child subcategory (41 classes) level occurred within the main categories (seven classes) for the urbanized and agriculture areas. It can be seen that some sporadic points are deviated from the diagonal line, but it still remains within the same square of the respective main land cover classes in Figure 4-3. Several urban land covers in the 41-classes-subcategory are buildings which are similar in appearance so making it difficult for the developed model to differentiate its usage, for example among apartment, industrial, and commercial buildings as shown in Figure 4-3, a-1, a-2, b-2 and b-2. Agricultural areas also include land cover sub-classes with similar outward shapes depending on consolidation that resulted in the misclassifications within the main category (Figure 4-3, a-3 and b-3).

However, grass and barren lands showed the wider misclassifications over the main land cover categories. Many of grass lands were misclassified by the forest, wetlands, and barren lands, of which appearances are similar as natural landscapes (Figure 4-3, a-4, a-5, b-4, b-5).

The statistics of 16 different perspective classifications are presented in Figure 4-4. As aforementioned, the final land cover classification was assigned statistically based on the maximum counts of a given land cover class.

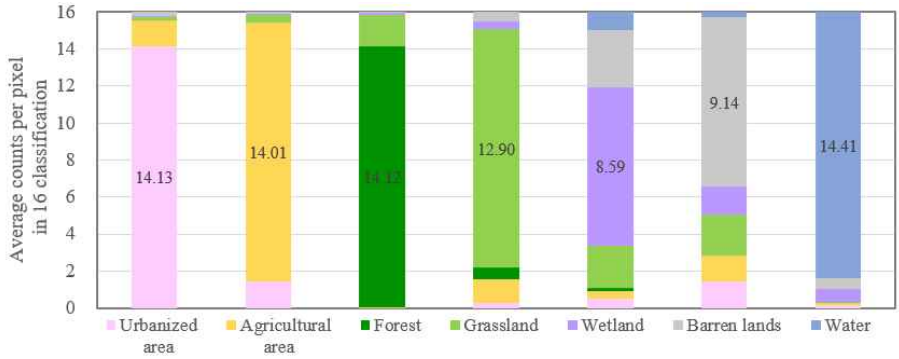

Figure 4-4. Average counts for different land covers from the 16 different perspective classifications (Park et al., 2020).

The greater the maximum count is, the more consistent the developed model performed for a given class. The average counts for urban, agriculture, forest, and water land covers were greater than 14, which indicates approximately 87% consistency of out of 16 classifications. This implies also that the consideration of viewpoints could improve classification consistency by reducing 13% potential errors as compared to a single-pixel based classification. Consistent with Figure 4-3, the maximum counts for wetland and barren lands were smaller than nine, which means nearly half of these categories could be misclassified as other land covers if the 16 different perspective classifications were not implemented. Thus the 16-perspective application can increase model accuracy by improving the model classification consistency.

4.4.2. Classification accuracy of the aggregated land cover to main category

The overall accuracy of the land cover classification was evaluated by expanding the printed land uses of child subcategory unit to the main category unit. A land cover map (Figure 4-5 (c)) of an orthographic image (Figure 4-5 (a)) of Subuk-myeon which is spatially and temporally similar to the study area (Jeonnam province, 2018) was printed through the land cover classification model developed in this study. This result is compared with the land cover map (Figure 4-5 (b)) obtained from EGIS and the accuracy metrics are presented in Table 4-5.

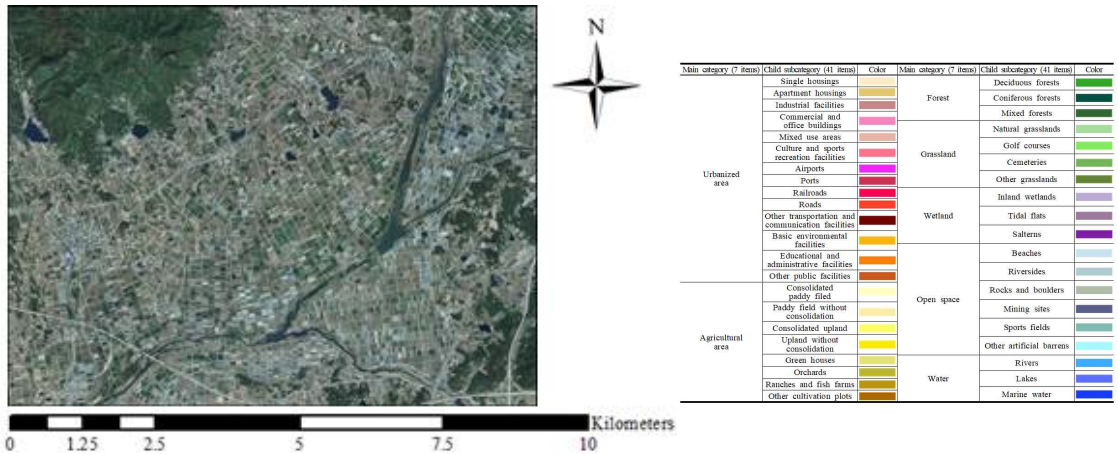

(a)

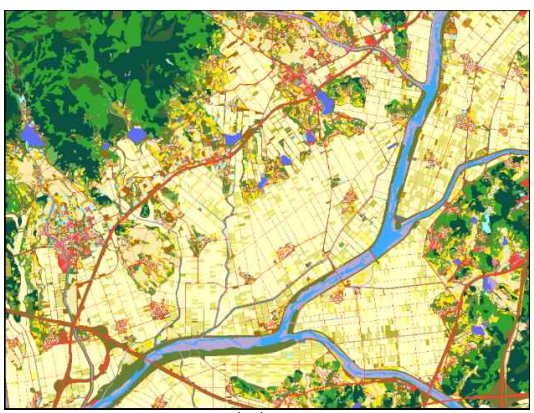

(b)

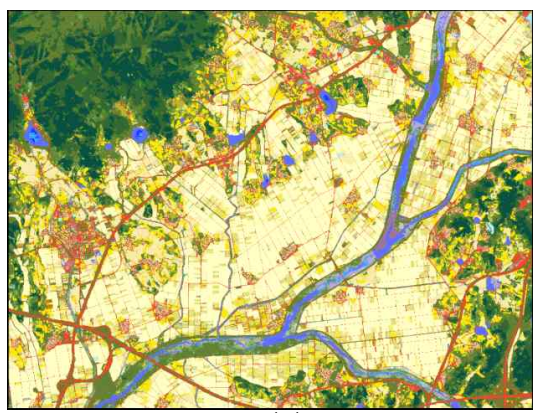

(c)

Figure 4-5 Photos of (a) Orthographic image, (b) land cover map, and (c) classification results of the Subuk-myeon area (Park et al., 2020).

Table 4-5. Accuracy metrics and verification indices for the Subuk-myeon area (unit: 1000 pixels) (Park et al., 2020).

		Classified Land Cover								Producer's Accuracy (%)
		Urbanized Area	Agricultural Area	Forest	Grassland	Wetland	Barren Lands	Water	Total	
Reference land cover	Urbanized area	18,658	2,834	19	1,850	41	193	24	23,619	79.0
	Agricultural area	4,439	114,426	61	5,848	177	1,122	114	126,187	90.7
	Forest	83	329	29,198	9,619	4	24	3	39,261	74.4
	Grassland	2,148	4,870	1414	23,920	424	853	43	33,672	71.0
	Wetland	138	309	22	3,840	1595	1,205	352	7,461	21.4
	Barren lands	1,369	802	13	879	13	385	9	3,469	11.1
	Water	29	22	1	153	688	187	5,055	6,133	82.4
	Total	26,864	123,593	30,728	46,108	2943	3,970	5,600	239,804	-
User's Accuracy (%)		69.5	92.6	95.0	51.9	54.2	9.7	90.3	-	-
Overall accuracy						0.81				
Kappa Value						0.71				

Visual comparison of both the land cover map of EGIS and the land cover map produced by the model shows an overall match between the two maps. However, the result showed large differences in the green areas of deciduous forests, coniferous forests, and mixed forests that were classified as the forest area. The classification of the overall forest area showed users accuracy of 95.02% and a producer's accuracy of 74.37%. This high accuracy result was achieved because the developed model is effective in classifying forest and other areas; however, it is not as effective in identifying detailed forest types within the forest area. As the forest area has large differences in elevations, the shades developed by its terrain, may affect the colors of the orthographic images. Such differences in colors made it difficult to classify the forests in detail.

The qualitative index of overall accuracy and kappa coefficient were 0.81 and 0.71, respectively. This showed a substantial degree of accuracy with the kappa coefficient $\geq$ 0.6 and < 0.8. It was confirmed that this was an improvement when compared to overall accuracy of 0.74 and kappa coefficient of 0.69 (Kim and Yeom, 2012) of the land cover classification using an object-based algorithm in the agricultural region.

Agricultural area, forest area and water showed high classification accuracy. The user's accuracy and producer's

accuracy of each classification item from the accuracy metrics showed in agricultural area (92.58%, 90.68%), forest area (95.0%, 74.4%), and water (90.3%, 82.4%), respectively. However, the classification accuracy of grassland (51.9%, 71.0%), wetlands (54.2%, 21.4%), and barren lands (9.7%, 11.1%) were low. It was caused by the misclassification of grassland to forest, wetland to grassland and barren lands, and barren lands to wetland and agricultural area.

This might be results from the ambiguity of the land cover, which causes difficulties in classification, as the forms of land uses are not clear (Figure 4-6 and 7).

(a) Orthographic image (b) Land cover map (c) Classification result

Figure 4-6. Example of ambiguity of land cover in grassland (yellowish green and whitish green is grass land, other greens are forest with different types of tree, yellows are agricultural area, and red is road) (Park et al., 2020).

Most of the forest area in the orthographic image (Figure 9 (a)) was defined as deciduous forest (Figure 4-6 (b), bright green) and coniferous forest (Figure 4-6 (b), dark green). However, the developed model classified mostly as mixed

forest (Figure 4-6 (c), intermediate dark green) and grass lands (Figure 4-6 (c), yellowish green). As mentioned, this might be due to difficulties of distinguish these two classes and thus more intensive training on forest areas are needed to increase the accuracy.

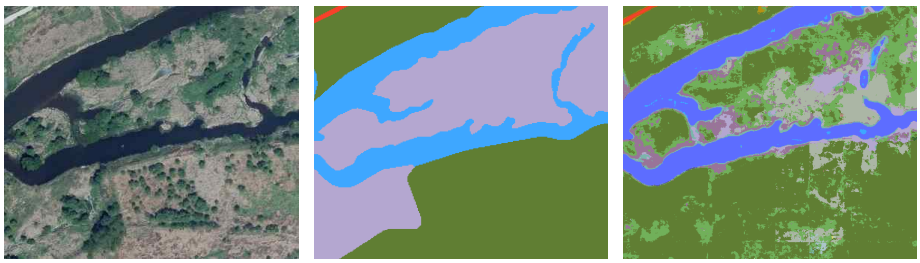

(a) Orthographic image (b) Land cover map (c) Classification result

Figure 4-7. Example of ambiguity of land cover in wetland and barren lands (purple is wetland, gray is barren lands, green is grass land, blue is river, red is road) (Park et al., 2020).

In the space surrounded by the central river of the orthographic image (Figure 4-7 (a)) near the river in Subuk-myeon, it is difficult to clearly classify the wetlands, barren lands, and grasslands by visual reading. In the land cover map (Figure 4-7 (b)) of EGIS, this was classified as a single land use (wetland) based on the land boundary, while in the land cover classification model, the classification of an optimal land use per pixel (Figure 4-7 (c)) was conducted. The differences in the land cover classification results caused by the ambiguity of the land cover largely affected the classification accuracy of wetlands and barren lands.

Wetlands are generally located in lower land area and thus pooled water during rainy season, while grasslands and barren lands are dry lands with and without vegetation, respectively. Thus wetlands, grasslands, and barren lands could share the similar landscape and its land cover changes depending on the existence of water and vegetation. This may have caused some ambiguity among those land covers that resulted in relatively poor performance. The ambiguity can be alleviated if additional indicators of NDWI (normalized difference water index) and NDVI (normalized difference vegetation index) are used, along with the RGB values.

Additionally, the overall portions of wetland and barren areas are relatively small as compared to other land covers, so the model might have been under-trained. The poor performance for water and barren area would be improved by training the model with more data specific to these land covers.

Figure 4-8 shows the orthographic image of Daeso-myeon (Figure 4-8 (a)), which is spatially (Chungbuk province) and periodically (2016) different from the study area (Jeonnam province, 2018) and the land cover map (Figure 4-8 (c)) classification produced by the land cover classification model. The accuracy metrics obtained by verifying it visually with the land cover map of EGIS (Figure 4-8 (b)) are presented in Table 4-6.

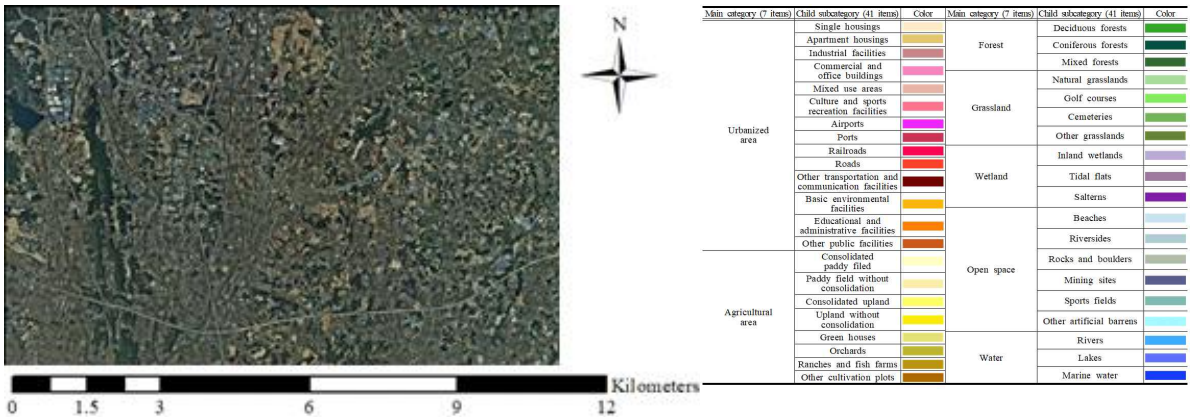

(**a**)

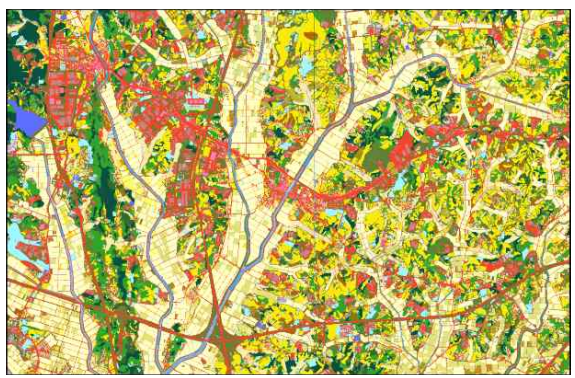

(**b**)

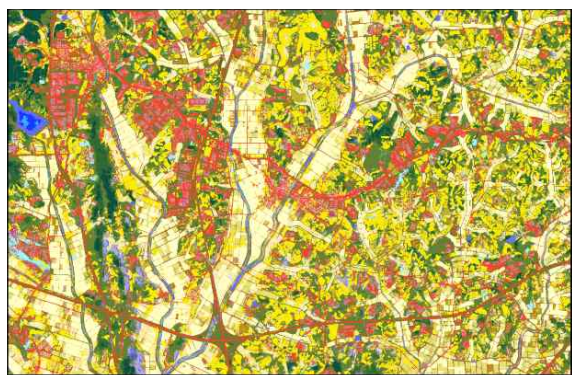

(**c**)

Figure 4-8. Photos of (a) Orthographic image, (b) land cover map, and (c) classification results of the Daeso-myeon area (Park et al., 2020).

Table 4-6. Accuracy metrics and verification indices of the Daeso-myeon area (unit: 1000 pixels) (Park et al., 2020).

		Classified Land Cover								Producer's Accuracy (%)
		Urbanized Area	Agricultural Area	Forest	Grassland	Wetland	Barren Lands	Water	Total	
Reference land cover	Urbanized area	44,614	4,451	25	4,026	203	334	68	53,721	83.1
	Agricultural area	6,759	124,749	254	6,677	334	737	402	139,912	89.2
	Forest	214	469	14,582	18,109	1,184	213	198	34,970	41.7
	Grassland	3,951	7,333	775	39,064	815	788	344	53,069	73.6
	Wetland	558	2,327	5	3,985	759	790	77	8,501	8.9
	Barren lands	3,956	3,483	14	2,702	131	2,280	38	12,604	18.1
	Water	73	321	2	378	280	249	2012	3,315	60.7
	Total	60,125	143,132	15,657	74,941	3,706	5,392	3139	306,093	-
User's Accuracy (%)		74.2	87.2	93.1	52.1	20.5	42.3	64.1	-	-
Overall accuracy						0.75				
Kappa Value						0.64				

Although the verification area was both spatially and periodically different from the study area, it was confirmed that the classification was conducted well when visually comparing the land cover map of EGIS with the land cover map produced by the model.

In particular, the qualitative index of overall accuracy and kappa coefficient were 0.75, and 0.64, respectively. When compared with the Subuk-myeon area (overall accuracy of 0.81, kappa coefficient of 0.71), which was similar to the study area, it showed approximately 10% lower accuracy. However, it showed a substantial degree of accuracy with kappa coefficient $\geq$ 0.6 and < 0.8. This result confirms the possibility of applying the land cover classification of a general orthographic image data regardless of its acquired time, or space. As for the classification accuracy of each item, the results for agricultural area (user's accuracy of 87.2%, producer accuracy of 89.2%) were accurate, whereas the results for wetlands (user's accuracy of 20.5%, producer's accuracy of 8.9%) and barren lands (user's accuracy of 42.3%, producer's accuracy of 18.1%) showed a lower level of accuracy. Thus, it can be confirmed that the results are similar to those from the aforementioned verification of Subuk-myeon.

In reality, the land uses of paddy field and upland are in the form of parcels with boundaries. However, the result of

the model produces the optimal land cover classification per pixel not per parcel with boundaries. As indicated by the red dotted lines shown in Figure 4-9, most of the area is classified as paddy field in the classification of a parcel of paddy field, whereas some part of the area is classified as upland. The ambiguity in boundaries could be improved to additional process of applying land parcel boundaries into pixel-based land cover.

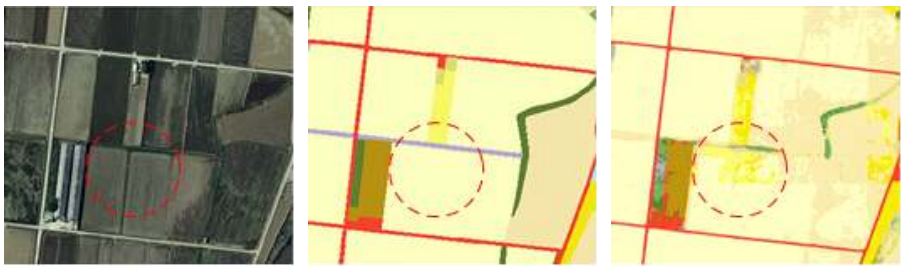

(a) Orthographic image (b) Land cover map (c) Classification result

Figure 4-9. Example of ambiguity of boundaries (bright and dark skin color are paddy field, bright and dark yellow are upland) (Park et al., 2020).

4.4.3. Classification accuracy of boundary based aggregation in agricultural area

The accuracy of extracted parcel boundary was evaluated by comparing the boundary separated from orthographic image using model and the farm map boundary, manually extracted parcel boundary. According to the interval of farm map production period, the most temporally closest data were used for validation. Orthographic images of 2018 and 2017 orthographic image based farm map were compared with Subuk-myeon and the same 2016 orthographic image based model result and farm map were validated on Daeso-myeon. The extracted boundary from the model (a), the parcel boundary of farm map (b), and verification image (c) and table (d) were shown in Figure 4-10 and 11, respectively.

(a)

(b)

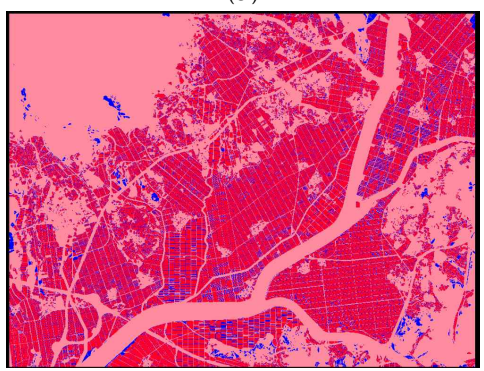

(c)

(1,000 pixel unit)		model	
		Positive	Negative
farm map	Positive	95,803	21,904
	Negative	175	121,922
Precision (%)		99.8	
Recall (%)		81.4	

(d)

Figure 4-10 Extracted agricultural parcel boundary in Subuk-myeon. (a) Farm map, (b) extracted boundary from post-processing module, (c) verification image of extracted boundary, and (d) verification table. Extracted agricultural area boundary was shown in white in (a)&(b). Accurately extracted boundaries were colored in red(TP for red, TN for pink) and mis-extracted boundaries were shown in blue(FP for sky blue, FN for blue).

(a)

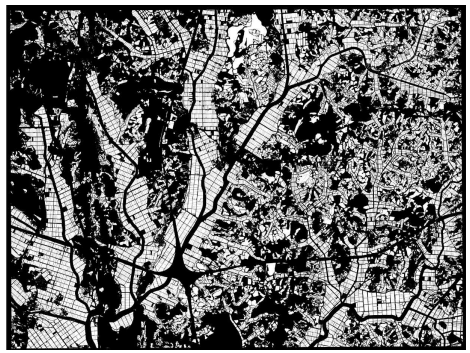

(b)

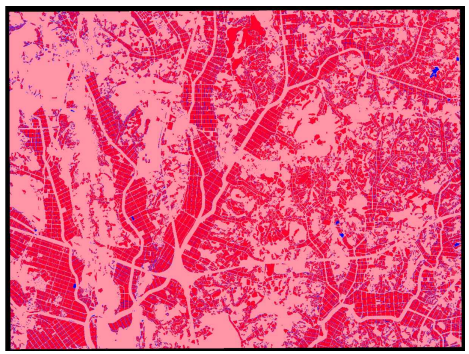

(c)

(1,000 pixel unit)		model	
		Positive	Negative
farm map	Positive	118,647	11,026
	Negative	2,701	173,719
Precision (%)		97.8	
Recall (%)		91.5	

(d)

Figure 4-11 Extracted agricultural parcel boundary in Daeso-myeon. (a) Farm map, (b) extracted boundary from post-processing module, (c) verification image of extracted boundary, and (d) verification table of Daeso-myeon. Extracted agricultural area boundary was shown in white in (a)&(b). Accurately extracted boundaries were colored in red(TP for red, TN for pink) and mis-extracted boundaries were shown in blue(FP for sky blue, FN for blue).

Precision, which predicts the accuracy among the extracted as parcel boundary by model, was accurately estimated on both verification area, larger than 97%. It confirms that the boundary extracted from model at least included in the real parcel boundary. However, recall, which means that how well the real boundaries could be extracted, showed low accuracy than precision though it was higher than 80%.

This result was caused by the differently set confines of parcel boundary between model and farm map. The space between lot and the lot was recognized as also lot in farm map (Figure 4-12 (b)), however, it was accepted as non-agricultural area in model result (Figure 4-12 (c)). It seems that the extracted boundary from model could represent the real parcel boundary in that the difference of parcel boundary mainly occurred on the edges of agricultural area.

(a) Orthographic image | (b) Agricultural boundary of farm map | (c) Extracted agricultural boundary

Figure 4-12 The example of extracted agricultural parcel boundary.

The recall of Subuk-myeon (81.4%) was lower than that of Daseo-myeon (91.5). The aggregation of land cover to parcel boundary module extracts the parcel boundary by detecting the change of gradient. The derivative of gradient was complicated near the mountain or river, which has diverse RGB even in small areas, and it resulted in the mis-extracted boundaries (Figure 4-13).

(a) Orthographic image (b) Agricultural boundary of farm map (c) Extracted agricultural boundary

Figure 4-13 The examples of mis-extracted parcel boundary near the mountain.

The accuracy of extracted parcel boundary from the model seemed well match with the farm map boundary, assigned as the real parcel boundary, regardless of spatially and timely. So, extracted boundary was applied to the previous CNN based land cover map to settle the ambiguity of boundaries (Figure 4-14, 4-15) and evaluated the land cover classification accuracy in agricultural area (Table 4-7&8, 9&10).

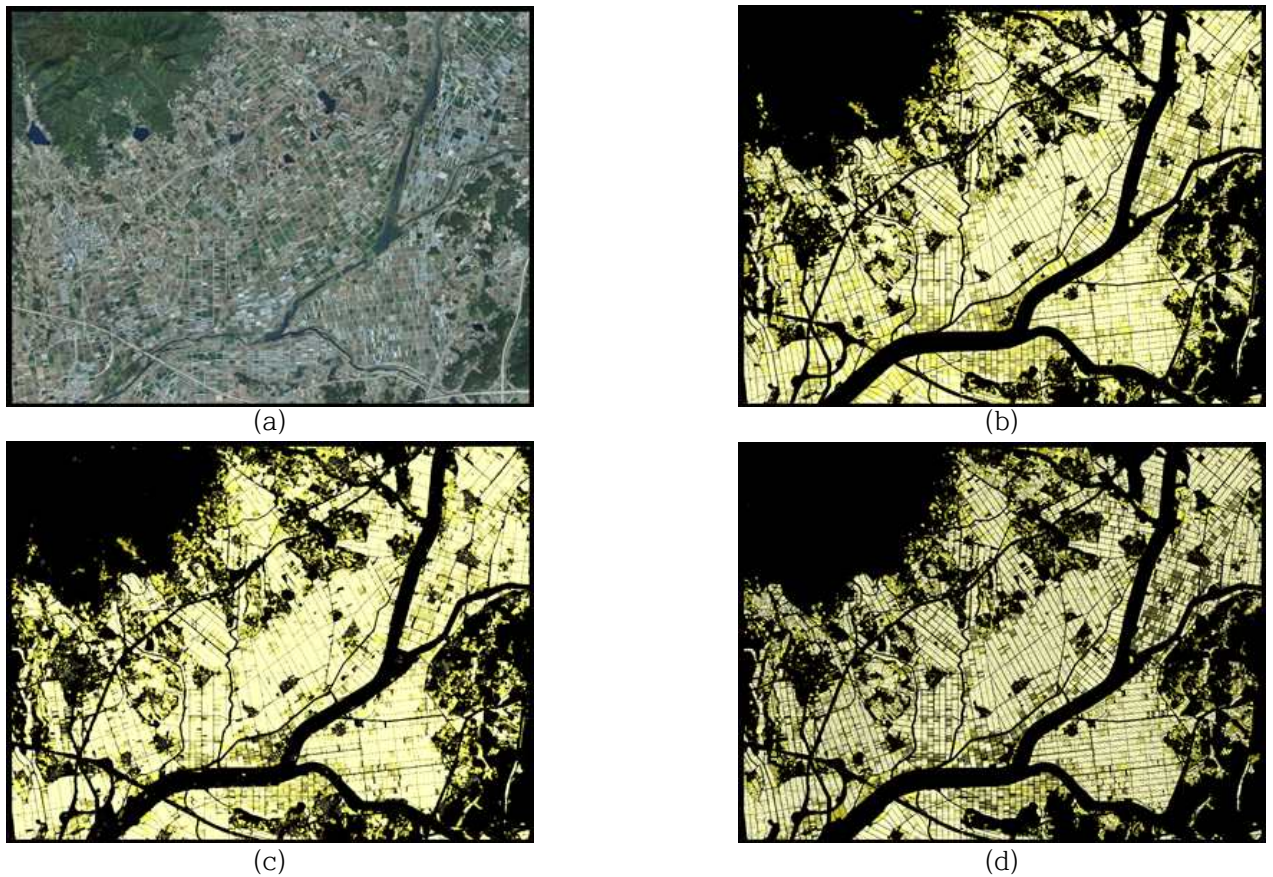

Figure 4-14 Agricultural land cover classification result in Subuk-myeon. (a) orthographic image (2018), (b) 2019 farm map(based on 2017 orthographic image), (c) pixel based classification result, and (d) boundary based classification result in agricultural area. Each color represent the land cover; Bright yellow for paddy; yellow for farm; green yellow for green house; brown for orchard.

Table 4-7 Accuracy metrics and verification indices of pixel based classification result in Subuk-myeon

(unit: 1.000.000 pixels)

		Classified Data (based on 2018 data)						Producer's accuracy (%)
		Paddy	Farm	Green house	Orchard	Others	Total	
Reference Data (based on 2017 data)	Paddy	66.6	5.3	1.8	0.1	2.4	76.2	87.4
	Farm	7.3	9.2	1.3	1.0	4.3	23.2	39.7
	Green house	1.4	0.6	9.4	0.1	1.7	13.1	71.2
	Orchard	0.3	1.0	0.3	1.4	2.2	5.3	26.6
	Others	6.8	3.0	4.5	2.2	105.6	122.0	86.5
	Total	82.5	19.0	17.3	4.9	116.2	239.8	-
User's accuracy (%)		80.7	48.4	54.1	28.7	90.9	-	-
Overall accuracy		0.80						
Kappa Value		0.69						

Table 4-8 Accuracy metrics and verification indices of pixel with boundary based classification result in Subuk-myeon.

(unit: 1.000.000 pixels)

		Classified Data (based on 2018 data)						Producer's accuracy (%)
		Paddy	Farm	Green house	Orchard	Others	Total	
Reference Data (based on 2017 data)	Paddy	58.0	4.7	1.1	0.6	11.8	76.2	76.2
	Farm	6.4	7.9	0.8	1.3	6.7	23.2	34.0
	Green house	0.9	0.5	7.0	0.0	4.7	13.1	53.4
	Orchard	0.4	1.0	0.1	1.2	2.6	5.3	22.4
	Others	0.5	0.2	0.3	0.1	121.0	122.0	99.2
	Total	66.2	14.3	9.4	3.1	146.8	239.8	-
User's accuracy (%)		87.7	55.0	75.0	37.4	82.4	-	-
Overall accuracy		0.81						
Kappa Value		0.69						

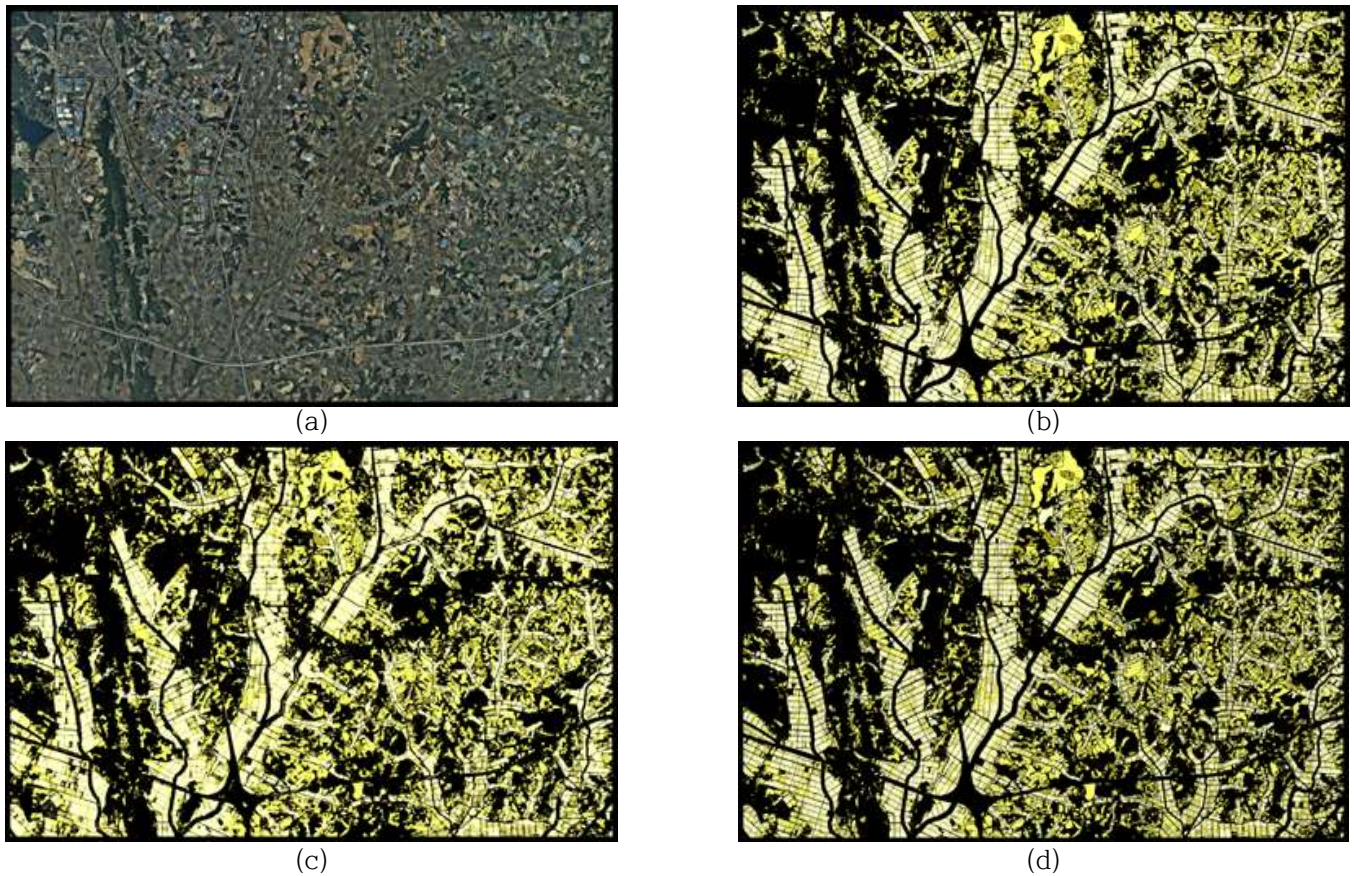

Figure 4-15 Agricultural land cover classification result in Daeso-myeon. (a) orthographic image (2016), (b) 2018 farm map(based on 2016 orthographic image), (c) pixel based classification result, and (d) boundary based classification result in agricultural area. Each color represent the land cover; Bright yellow for paddy; yellow for farm; green yellow for green house; brown for orchard.

Table 4-9 Accuracy metrics and verification indices of pixel based classification result in Daeso-myeon

(unit: 1.000.000 pixels)

		Classified Data (based on 2016 data)						Producer's accuracy (%)
		Paddy	Farm	Green house	Orchard	Others	Total	
Reference Data (based on 2016 data)	Paddy	53.9	7.5	0.6	0.1	0.8	63.0	85.6
	Farm	2.5	36.5	0.8	1.8	7.4	49.0	74.4
	Green house	0.4	0.5	11.5	0.4	3.1	15.9	72.4
	Orchard	0.0	0.2	0.1	1.4	1.2	2.9	47.8
	Others	7.0	7.3	6.5	4.1	150.5	175.3	85.8
	Total	63.9	52.0	19.6	7.7	163.0	306.1	-
User's accuracy (%)		84.5	70.2	58.8	18.1	92.3	-	-
Overall accuracy		0.83						
Kappa Value		0.72						

Table 4-10 Accuracy metrics and verification indices of pixel with boundary based classification result in Daeso-myeon.

(unit: 1.000.000 pixels)

		Classified Data (based on 2016 data)						Producer's accuracy (%)
		Paddy	Farm	Green house	Orchard	Others	Total	
Reference Data (based on 2016 data)	Paddy	49.5	6.8	0.1	0.2	6.4	63.0	78.6
	Farm	2.2	35.9	0.4	4.4	6.2	49.0	73.2
	Green house	0.2	0.5	13.4	0.1	1.6	15.9	84.6
	Orchard	0.0	0.2	0.1	2.3	0.3	2.9	79.7
	Others	1.8	2.1	0.5	0.5	170.4	175.3	97.2
	Total	53.7	45.4	14.5	7.5	185.0	306.1	-
User's accuracy (%)		92.1	79.1	92.5	31.3	92.1	-	-
Overall accuracy		0.89						
Kappa Value		0.81						

Estimated verification indices of overall accuracy and kappa value were 0.81 and 0.69 in Subuk-myeon, 0.89 and 0.8 in Daeso-myeon, respectively. The overall accuracy was advanced 0.80 to 0.81 in Subuk-myeon and 0.83 to 0.89 in Daeso-myeon. Aggregation of land cover based on extracted parcel boundary led to not only the accuracy improvement but also express actual land use.

In Subuk-myeon, the user's accuracy was overall improved, but overall accuracy improved only 1% and the producer's accuracy of greenhouse decreased 71.2% to 53.4%. Timely difference between ground truth (2017 orthographic image based 2019 farm map) and model result (based on 2018 orthographic image) caused the inaccurate comparison. Figure 4-16 represents the changed land use in agricultural area within one year; removed greenhouse in red circle and created greenhouse in blue circle. The latest farm map of 2019, delayed due to the manual process, could provide inaccurate land cover and the capability of developed model, extracting land cover immediately from orthographic image, could be effectively applied to extracting real-time agricultural land cover.

(a) Orthographic image (2018)

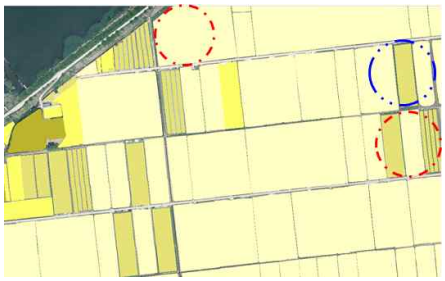

(b) Farm map (2017)

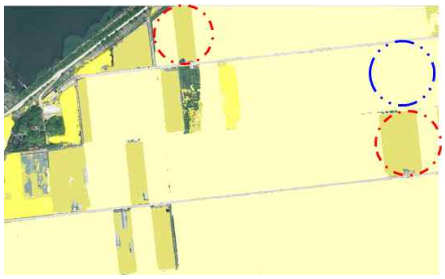

(c) Pixel based land cover classification result (2018)

(d) Pixel with boundary based land cover classification result (2018)

Figure 4-16 The land cover classification result comparison in Subuk-myeon.

Daeso-myeon, where the ground truth of farm map and result of developed model land cover classification were same in 2016, showed high accuracy with overall accuracy of 0.89 and 'almost perfect' level kappa coefficient, which is the highest level of accuracy with a kappa coefficient of over 0.8.

The land cover that was classified into several land use in each pixel were aggregated to one land cover (Figure 4-17 red circle) based on the extracted parcel boundary or removed (Figure 4-17 blue circle).

Extracted paddy and farm from developed model were more accurate compared to pixel based result, through the

increase of the user's accuracies. However, the actual paddy and farm from the ground truth farm map were less extracted with the decrease of producer's accuracy. This is the result of the boundary extraction module that does not classify the spaces between lots as agricultural parcels (Figure 4-16 (b) & (d) and Figure 4-17 (b) & (d).

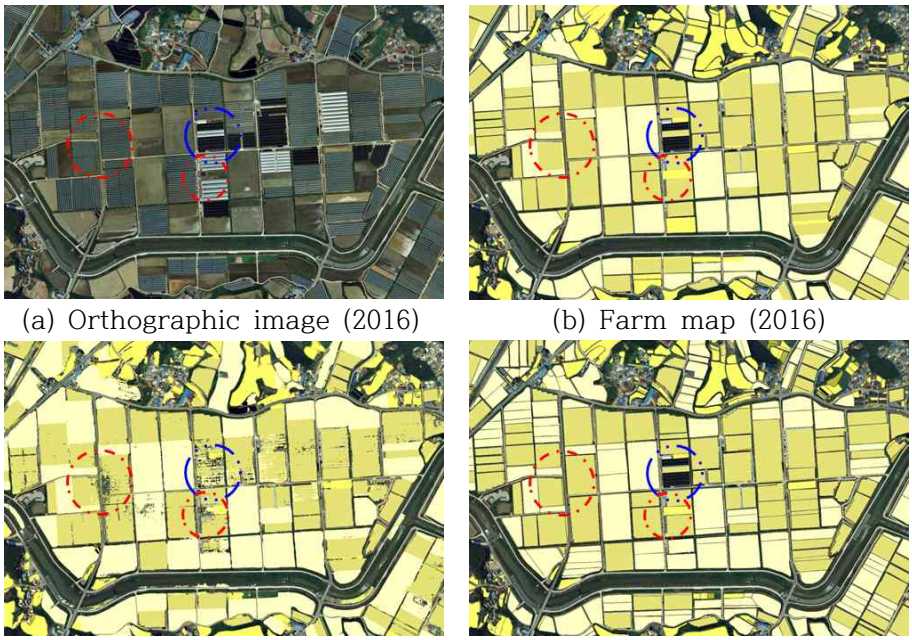

(a) Orthographic image (2016)
(b) Farm map (2016)
(c) Pixel based land cover classification result (2016)
(d) Pixel with boundary based land cover classification result (2016)

Figure 4-17 The land cover classification result comparison in Daeso-myeon

Though producer's accuracy of paddy and farm have slightly decreased (paddy 7.0% and farm 1.2%), Other accuracies of each land cover increased by 17.9% on average. Especially, the accuracy of greenhouse was greatly enhanced with 12.2% of producer's accuracy and 33.7% of

user's accuracy. It could be confirmed that the agricultural land cover was accurately extracted using developed model compare to farm map, which created from time consuming and labor intensive on-digitizing method.

Additionally, land cover classification was conducted using an objective workstation of commercial software ERDAS Imagine (Figure 4-18, Table 4-11) and compared the accuracy with the developed model result to review the applicability of developed model in agricultural classification.

The result of agricultural classification using ERDAS Imagine showed that both user's accuracy and producer's accuracy were low with an average of 34.4% and 23.5%. In particular, paddy was misclassified as farm and farm as paddy, and greenhouse&orchard were misclassified as others, mainly to roads and forests&grasslands, respectively. It can be seen that the characteristic of ERDAS Imagine, which assign a land cover label based on a DN in each pixel, caused misclassification on the area of similar color values. Moreover, the difference between objects grouped using ERDAS Imagine and actual boundaries deteriorated the accuracy.

This implies that the developed model is particularly applicable to parcel-level agricultural cover classification compared to ERDAS Imagine specialized in main category cover classification.

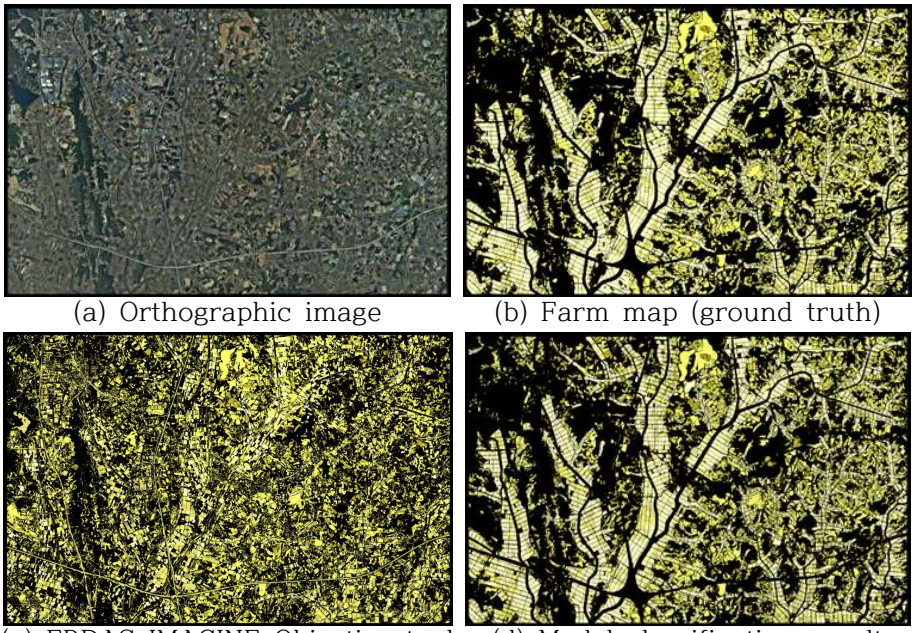

(a) Orthographic image (b) Farm map (ground truth)

(c) ERDAS IMAGINE Objective tool (d) Model classification result (Pixel with boundary based result)

Figure 4-18 Comparison of the agricultural cover classification results in Daeso-myeon. (Bright yellow for paddy, yellow for farm, green yellow for green house, brown for orchard, and black for others.)

Table 4-11 Accuracy metrics and verification indices of ERDAS Imagine result with farm map in Daeso-myeon.

(unit: 1.000.000 pixels)

		ERDAS IMAGEINE result						Producer's accuracy (%)
		Paddy	Farm	Green house	Orchard	Others	Total	
Farm map	Paddy	8.9	10.2	3.8	9.6	29.1	61.7	14.4
	Farm	0.4	13.9	6.2	5.0	22.3	47.8	29.1
	Green house	0.3	1.9	0.5	7.5	5.0	15.3	3.5
	Orchard	0.0	0.2	0.6	0.2	1.9	2.9	6.5
	Others	2.7	19.5	11.0	31.5	113.7	178.4	63.7
	Total	12.3	45.8	22.2	53.9	172.0	306.1	-
User's accuracy (%)		72.7	30.4	2.4	0.3	66.1	-	-
Overall accuracy		0.45						
Kappa Value		0.13						

Chapter 5. Conclusions

As an effort to improve the update of land cover maps especially for agriculture, this study developed the land cover classification model using the CNN-based FusionNet network structure and advanced the developed model accuracy in agricultural areas by applying parcel boundary extraction algorithm. The developed model verified its applicability for the two areas of different spatial and temporal characteristics.

The developed model was designed to classify land cover from orthographic images by considering spatial distributions of each pixel using CNN structure and reading 16 images of different perspectives to classify a single area. The classification consistency was increased by approximately 87%.

Performance of the developed model was reasonably good demonstrating the overall accuracies of 0.81 and 0.75, and kappa coefficients of 0.71 and 0.64, respectively. However, wetlands and barren lands were substantially misclassified to grassland and wetland which were trained with relatively small area. Thus, further training with data specific to these land covers may improve accuracy.

When considering parcel boundaries in agricultural area,

the model performance showed overall accuracy of 0.89 and kappa coefficients of 0.81, which grade the highest level of ‘almost perfect’. Aggregation of land cover in pixel to parcel boundary led to not only the accuracy improvement but also expressed actual land use.

It was concluded that the developed model could assist the current slow process of land cover classification, especially on parcel-level agricultural cover classification. Since the developed model was based on CNN, maintenance such as continuous model training with the future land cover information is required to sustainable model performance. Additionally, produced near real-time land cover maps could enhance the accuracy of model simulation for watershed and land use change, and thus it will be future studies.

Reference

1. Anderson, M.C., R.G. Allen, A. Morse and W. Kustas, 2012. Use of Landsat thermal imagery in monitoring evapotranspiration and managing water resources. Remote Sens. Environ. 122, pp. 50-65.
2. Barazzetti, L., R. Brumana, D. Oreni, M. Previtali and F. Roncoroni, 2014. True-orthophoto generation from UAV images: Implementation of a combined photogrammetric and computer vision approach. ISPRS Annals of the Photogrammetry, Remote Sensing and Spatial Information Sciences. 23-25 June 2014, Riva del Garda, Italy, 2(5), pp. 57-63.
3. Blasi, C., L. Zavattero, M. Marignani, D. Smiraglia, R. Copiz, L. Rosati and E. Del Vico, 2008. The concept of land ecological network and its design using a land unit approach. Plant Biosyst. 142(3), pp. 540-549.
4. Bontemps, S., M. Arias, C. Cara, G. Dedieu, E. Guzzonato, O. Hagolle, J. Inglada, N. Matton, D. Morin, R. Popescu, et al. 2015. Building a data set over 12 globally distributed sites to support the development of agriculture monitoring applications with Sentinel-2. Remote Sens. 7(12), pp. 16062-16090.
5. Borrelli, P., D.A. Robinson, L.R. Fleischer, E. Lugato, C. Ballabio, C. Alewell and V. Bagarello, 2017. An assessment of the global impact of 21st century land use change on soil erosion. Nat. Commun. 8(1), pp. 1-13.
6. Carranza-García, M., J. García-Gutiérrez and J. Riquelme, 2019. A framework for evaluating land use and land cover classification using convolutional neural networks. Remote

Sens. 11(3), pp. 274.
7. Chen, Y., Z. Lin, X. Zhao, G. Wang and Y. Gu, 2014. Deep learning-based classification of hyperspectral data. IEEE J. Sel. Top. Appl. Earth Obs. Remote. Sens. 7(6), pp. 2094-2107.
8. Cho, S.M. and K.K. Oh, 2004. Classification of Warm Temperate Vegetation Using Satellite Data and Management System. Korean Journal of Environment and Ecology , 18(2), pp. 231-235.
9. Cho, Y.S., N.Y. Lim, W.S. Joung, S.H. Jung and S.K. Choi, 2014. Management of construction fleds information using low altitude close-range aerial images. Journal of the Korean Society of Surveying, Geodesy, Photogrammetry and Cartography. 32(5), pp. 551-560.
10. Choi, G.Y. and S.K, Kang, 2010. Estimation of carbon assimilation volume change in Korea using MODIS satellite image. The Korean Geographical Society. Pp. 27-30.
11. Choi, C.H., S.G, Jung, G.H. Park and G.T. Kim, 2015. Analysis of plant season change and assesment of climate influence using satellite image. Proceedings of the Korean Institute of Landscape Architecture Conference. 2015, pp. 100.
12. Çiçek, Ö., A. Abdulkadir, S.S. Lienkamp, T. Brox and O. Ronneberger, 2016. 3D U-Net: Learning dense volumetric segmentation from sparse annotation. In Proceedings of the International Conference on Medical Image Computing and Computer-Assisted Intervention, Athens, Greece, 17-21 Volume 9901, pp. 424-432.
13. Da Costa, J.P., F. Michelet, C. Germain, O. Lavialle, and G. Grenier. 2007. Delineation of Vine Parcels by

Segmentation of High Resolution Remote Sensed Images. Precision Agriculture 8 (1-2), pp. 95-110. doi:10.1007/s11119-007-9031-3.

14. Enderle, D.I. and R.C. Weih Jr, 2005. Integrating supervised and unsupervised classification methods to develop a more accurate land cover classification. Journal of the Arkansas Academy of Science. 59(1), pp. 65-73.
15. Fu, G., C. Liu, R. Zhou, T. Sun and Q. Zhang, 2017. Classification for high resolution remote sensing imagery using a fully convolutional network. Remote Sens. 9(5), pp. 498.
16. García-Pedrero, A., C. Gonzalo-Martín and M. Lillo-Saavedra, 2017. A machine learning approach for agricultural parcel delineation through agglomerative segmentation. International journal of remote sensing. 38(7), pp. 1809-1819.
17. Gavade, A.B. and V.S. Rajpurohit, 2019. Systematic analysis of satellite image-based land cover classification techniques: Literature review and challenges. Int. J. Comput. Appl. pp. 1-10. doi:10.1080/1206212x.2019.1573946.
18. Grinblat, G.L., L.C. Uzal, M.G. Larese and P.M. Granitto, 2016. Deep learning for plant identification using vein morphological patterns. Comput. Electron. Agric. 127, pp. 418-424
19. Hagen, N. and E. L. Dereniak, 2008. Gaussian Profile Estimation in Two Dimensions. Appl. Opt. 47(36), pp. 6842-6851. doi: 10.1364/AO.47.006842.
20. He, T., Q. Shao, W. Cao, L. Huang and L. Liu, 2015. Satellite-observed energy budget change of deforestation in northeastern China and its climate implications.

Remote Sens. 7(9), pp. 11586-11601.
21. Huang, X. and L. Zhang, 2012. An SVM ensemble approach combining spectral, structural, and semantic features for the classification of high-resolution remotely sensed imagery. IEEE Trans. Geosci. Remote Sens. 51(1), pp. 257-272.
22. Jin, B., P. Ye, X. Zhang, W. Song and S. Li, 2019. Object-oriented method combined with deep convolutional neural networks for land-use-type classification of remote sensing images. J. Indian Soc. Remote Sens. 47(6), pp. 951-965.
23. Kamilaris, A. and F.X. Prenafeta-Boldú, 2018, A review of the use of convolutional neural networks in agriculture. J. Agric. Sci. 156, pp. 312-322.
24. Kang, M. S., S. W. Park and S. Y. Kwang, 2006. Land cover classification of image data using artificial neural networks. Journal of Korean Society of Rural Planning. 12(1), pp. 75-83.
25. Kang, N.Y., J.G. Pak, G.S. Cho and Y. Yeu, 2012 An analysis of land cover classification methods using IKONOS satellite image. J. Korean Soc. Geospat. Inf. Syst. 20(3), pp. 65-71.
26. Kim, J.N. and D,Y. Um, 2015. High quality ortho-image production using the hisgh resolution DMC Ⅱ aerial image. Journal of the Korean Society of Surveying, Geodesy, Photogrammetry and Cartography. 33(1), pp. 11-21. (in Korean with English abstract)
27. Kim, H.O. and J.M. Yeom, 2012. A study on object-based image analysis methods for land cover classification in agricultural areas. J. Korean Assoc. Geogr. Inf. Stud. 15, pp. 26-41.

28. Kim, H.J., D.Y. Han and Y.I. Kim, 2006. Building height extraction using triangular vector structure from a single high resolution satellite image. Korean Journal of Remote Sensing. 22(6), pp. 621-626.
29. Cultivated area by city and county in 2017 from Kostat total survey of agriculture, forestry and fisheries. Available online: http://kosis.kr/statHtml/statHtml.do?orgId=101&tblId=DT_1EB002&conn_path=I2 (27 September 2020)
30. Kussul, N., M. Lavreniuk, S. Skakun and A. Shelestov, 2017. Deep learning classification of land cover and crop types using remote sensing data. IEEE Geosci. Remote Sens. Lett. 14(5), pp. 778-782.
31. Laha, A., N.R. Pal and J. Das, 2006. Land cover classification using fuzzy rules and aggregation of contextual information through evidence theory. IEEE Transactions on Geoscience and Remote Sensing. 44(6), pp. 1633-1641.
32. Lakhwani, K., P. D. Murarka and N. S. Chauhan, 2015. Color Space Transformation for Visual Enhancement of Noisy Color Image. International Journal of ICT and Management. 3(2), pp. 9-13.
33. Landis, J.R. and G.G. Koch, 1977. The measurement of observer agreement for categorical data. Biometrics. 33, pp. 159-174.
34. Längkvist, M., A. Kiselev, M. Alirezaie and A. Loutfi, 2016. Classification and segmentation of satellite orthoimagery using convolutional neural networks. Remote Sens. 8(4), pp. 329.
35. Lee, H.J., J.H. Lu and S.Y. Kim, 2011. Land Cover Object-oriented Base Classification Using Digital Aerial

Photo Image. Journal of Korean Society for Geospatial Information System 19(1), 2011.3, 105-113(9 pages)
36. Lee, S.H., C.S. Chan, P. Wilkin and P. Remagnino, 2015. Deep-plant: Plant identification with convolutional neural networks. In Proceedings of the 2015 IEEE International Conference on Image Processing (ICIP), Quebec City, QC, Canada, pp. 27-30.
37. Lee, D. Y., D. K. Shin and D. I. Shin, 2016. A Finger Counting Method for Gesture Recognition. Journal of Internet Computing and Services. 17(2), pp. 29-37. doi: 10.7472/jksii.2016.17.2.29. (in Korean)
38. Lu, H., X. Fu, C. Liu, L.-G. Li and Y.-X. He, 2017. Cultivated land information extraction in UAV imagery based on deep convolutional neural network and transfer learning. J. Mt. Sci. 14(4), pp. 731-741.
39. Luus, F.P.S., B.P. Salmon, F.V.D. Bergh and B.T. Maharaj, 2015. Multiview deep learning for land-use classification. Ieee Geosci. Remote Sens. Lett. 12(12), pp. 2448-2452.
40. Mueller, M., S. Karl and H. Kaufmann, 2004. Edge- and region-based segmentation technique for the extraction of large, man-made objects in high-resolution satellite imagery. Patter Recognition 37(8), pp. 1619-1628.
41. Na, S.I., C.W. Park, K.H. So, H.Y. Ahn and K.D. Lee, 2019. Selection on optimal bands to estimate yield of the Chinese cabbage using drone-based hypersperctral image. Korean Journal of Remote Sensing, 35(3), pp. 375-387
42. Oh, S.H., K.H. Jang and S.K, Jung, 2008. A semi-automatic building modeling system using a single satellite image. The KIPS Transactions : Part B, 16(6), pp. 451-462.
43. Otsu, N., 1979. A Threshold Selection Method from

Gray-Level Histograms. IEEE Trans. Syst. Man Cybern. 9(1), pp. 62-66. doi: 10.1109/TSMC.1979.4310076.
44. Paisitkriangkrai, S., C. Shen and H. Av, 2016, Pedestrian detection with spatially pooled features and structured ensemble learning. IEEE Trans. Pattern Anal. Mach. Intell. 38(6), pp. 1243-1257.
45. Pan, S., H. Guan, Y. Chen, Y. Yu, W. Gonçalves, J.M. Junior and J. Li, 2020. Land-cover classification of multispectral LiDAR data using CNN with optimized hyper-parameters. ISPRS J. Photogramm. Remote Sens. 166, pp. 241-254.
46. Park, J.K. and J.S. Lee, 2017. Analysis of Abnormal High Temperature Phenomena in Cixi-si of China using Landsat Satellite Images. Korea Academy Industrial Cooperation Society. 18(8), pp. 34-40.
47. Park, J.S., S.J. Jang, R.G. Hong, K. Suh, and I.H. Song, 2020. Development of Land Cover Classification Model Using AI Based FusionNet Network. Remote Sens. 2020, 12(19), 3171.
48. Park, J.H., K.W. Park and I.G. Jung, 2018. Bias Correction of Gridded Climate Data based on Satellite Imagery. Korean Society of Civil Engineers. pp. 32-33
49. Prasad, S.V.S., T.S. Savitri and I.V.M. Krishna, 2011. Classification of multispectral satellite images using clustering with SVM classifier. Int. J. Comput. Appl. 35(5), pp. 32-44.
50. Phiri, D. and J. Morgenroth, 2017. Developments in Landsat land cover classification methods: A review. Remote Sensing 9.9: 967.
51. Quan, T.M., D.G. Hildebrand and W.K. Jeong, 2016. Fusionnet: A deep fully residual convolutional neural

network for image segmentation in connectomics. arXiv 2016, arXiv:1612.05360.
52. Rabiu, L. and D.A. Waziri, 2014. Digital orthophoto generation with aerial photograph. Academic Journal of Interdisciplinary Studies. 3(7), pp. 133-141
53. Rahman, S. 2010. Six decades of agricultural land use change in Bangladesh: Effects on crop diversity, productivity, food availability and the environment, 1948-2006. Singap. J. Trop. Geogr. 31(2), pp. 254-269.
54. Richard, O. D. and Peter, E. H. Use of the Hough transformation to detect lines and curves in pictures. Commun. ACM 1971, 15(1), pp. 11-15. doi: 10.1145/361237.361242.
55. Ronneberger, O., P. Fischer and T. Brox, 2015. U-net: Convolutional networks for biomedical image segmentation. In International Conference on Medical Image Computing and Computer-Assisted Intervention. Springer, cham, pp. 234-241.
56. Roy, M., F. Melgani, A. Ghosh, E. Blanzieri and S. Ghosh, 2015. Land-cover classification of remotely sensed images using compressive sensing having severe scarcity of labeled patterns. IEEE Geosci. Remote Sens. Lett. 12(6), pp. 1257-1261
57. Sakong, H. and J. Im, 2003. An empirical study on the land cover classification method using IKONOS image. Journal of the Korean Association of Geographic Information Studies. 6(3), pp. 107-116.
58. Santoni, M.M., D.I. Sensuse, A.M. Arymurthy and M.I. Fanany, 2015. Cattle race classification using gray level co-occurrence matrix convolutional neural networks. Procedia Comput. Sci. 59, pp. 493-502.

59. Schilling, K.E., M.K. Jha, Y.K. Zhang, P.W. Gassman and C.F. Wolter, 2008. Impact of land use and land cover change on the water balance of a large agricultural watershed: Historical effects and future directions. Water Resour. Res. 44(7)
60. Schöpfer, E., S. Lang and J. Strobl, 2010. Segmentation and object-based image analysis. Remote Sensing of Urban and Suburban Areas. pp. 181-192.
61. Segl, K. and H. Kaufmann, 2001. Detection of small objects from high-resolution panchromatic satellite imagery based on supervised image segmentation. IEEE transactions on geoscience and remote sensing, 39(9), pp. 2080-2083.
62. Shang, W., K. Sohn, D. Almeida and H. Lee, 2016. Understanding and improving convolutional neural networks via concatenated rectified linear units. In International Conference on Machine Learning, pp. 2217-2225.
63. Shin, J.S., T.H. Lee, P.M. Jung and H.S. Kwon, 2015. A Study on Land Cover Map of UAV Imagery using an Object-based Classification Method. Journal of Korean Society for Geospatial Information System 23(4), 2015.12, 25-33(9 pages)
64. Shimrat, M., 1962. Algorithm 112: Position of Point Relative to Polygon. Commun. ACM. 5(8), pp. 434. doi: 10.1145/368637.368653.
65. Suzuki, S. and K. Abe, 1985. Topological Structural Analysis of Digitized Binary Images by Border Following. Computer Vision, Graphics, and Image Processing. 30(1), pp. 32-46. doi: 10.1016/0734-189X(85)90016-7.
66. Turker, M. and E. H. Kok, 2013. Field-based

sub-boundary extraction from remote sensing imagery using perceptual grouping. Jouranal of Photogrammetry and Remote Sensing 79, pp. 106-121

67. Waldner, F. and F. I. Diakogiannis, 2020. Deep learning on edge: Extracting field boundaries from satellite images with a convolutional neural network. Remote sensing of environment. 245, p.111741.
68. Yan, L. and D. P. Roy, 2014. Automated Crop Field Extraction from Multi-temporal Web Enabled Landsat Data. Remote Sensing of Environment 144, pp. 42-64.
69. Yang, J., F. Chen, J. Xi, P. Xie and C. Li, 2014. A multitarget land use change simulation model based on cellular automata and its application. Abstr. Appl. Anal. 2014. pp. 1-11
70. Yeom, J.H. and Y.I. Kim, 2014. Automatic extraction of the land readjustment paddy for high - level land cover classification. Journal of the Korean Society of Surveying, Geodesy, Photogrammetry and Cartography 32(5), pp. 443-450.
71. Yoo, Y.H., J.W. Choi, S.K. Choi and S.H. Jung, 2016. Quality evaluation of orthoimage and DSM based on fixed-wing UAV corresponding to overlap and GCPs. Journal of the Korean Society for Geospatial Information Science. 24(3), pp. 3-9. (in Korean with English abstract)
72. Zeiler, M.D. and R. Fergus, 2013. Stochastic pooling for regularization of deep convolutional neural networks. arXiv 2013, arXiv:1301.3557.

국 문 초 록

토지이용이 빠르게 변화함에 따라, 토지 피복에 대한 공간정보를 담고 있는 토지 피복 지도의 신속한 최신화는 필수적이다. 하지만, 현 토지 피복 지도는 많은 시간과 노동력을 요구하는 manual digitizing 방법으로 제작됨에 따라, 토지 피복 지도의 업데이트 및 배포에 긴 시간 간격이 발생하는 실정이다. 본 연구에서는 convolutional neural network (CNN) 기반의 인공신경망을 이용하여 high-resolution remote sensing (HRRS) 영상으로부터 토지 피복을 분류하는 모델을 개발하고, 특히 농지 경계추출 알고리즘을 적용하여 농업지역에서 분류 정확도를 개선하고자 하였다. 개발된 토지 피복 분류모델은 전처리(pre-processing) 모듈, 토지 피복 분류(land cover classification) 모듈, 그리고 후처리(post-processing) 모듈의 세 모듈로 구성된다. 전처리 모듈은 입력된 HRRS 영상을 75%씩 중첩 분할하여 관점을 다양화하는 모듈로, 한 관점에서 토지 피복을 분류할 때 발생할 수 있는 오분류를 줄이고자 하였다. 토지 피복 분류 모듈은 FusionNet model 구조를 바탕으로 개발되었고, 이는 분할된 HRRS 이미지의 픽셀별로 최적 토지 피복을 부여하도록 설계되었다. 후처리 모듈은 픽셀별 최종 토지 피복을 결정하는 모듈로, 분할된 HRRS 이미지의 분류결과를 취합하여 최빈값을 최종 토지 피복으로 결정한다. 추가로 농지에서는 농지경계를 추출하고, 필지별 분류된 토지 피복을 집계하여 한 필지에 같은 토지 피복을 부여하였다. 개발된 토지 피복 분류모델은 전라남도 지역(면적: 547 km^2)의 2018년 정사영상과 토지 피복 지도를 이용하여 학습되었다. 토지 피복 분류모델

검증은 학습지역과 시간, 공간적으로 구분된, 2018년 전라남도 수북면과 2016년 충청북도 대소면의 두 검증지역에서 수행되었다. 각 검증지역에서 overall accuracy는 0.81, 0.71로 집계되었고, kappa coefficients는 0.75, 0.64로 산정되어 substantial 수준의 토지 피복 분류 정확도를 확인하였다. 특히, 개발된 모델은 필지 경계를 고려한 농업지역에서 overall accuracy 0.89, kappa coefficient 0.81로 almost perfect 수준의 우수한 분류 정확도를 보였다. 이에 개발된 토지 피복 분류모델은 특히 농업지역에서 현 토지 피복 분류 방법을 지원하여 토지 피복 지도의 빠르고 정확한 최신화에 기여할 수 있을 것으로 생각된다.

주요어: 토지 피복 지도, 토지 피복 분류, 합성곱 신경망, 필지 경계

학 번: 2019-26400